· Article · Advances in Polar Science
doi: 10.12429/j.advps.2023.0002 September 2023 Vol. 34 No. 3: 190-219

Performance of surface radiation products of Greenland Ice Sheet using in-situ measurements

CHE Jiahang[1], HUAI Baojuan[1*], SUN Weijun[1], DING Minghu[2], WANG Lei[1], ZHANG Qinglin[1], WU Jiake[1], KANG Limin[1], TENG Xinru[1], YANG Xiaohong[1], YAN Jinpei[3] & ZHAO Shuhui[4]

[1] College of Geography and Environment, Shandong Normal University, Jinan 250358, China;
[2] State Key Laboratory of Severe Weather, China Academy of Meteorological Sciences, Beijing 100081, China;
[3] Key Laboratory of Global Change and Marine-Atmospheric Chemistry, Third Institute of Oceanography, Ministry of Natural Resources, Xiamen 361005, China;
[4] School of Tourism, Taishan University, Taian 271021, China

Received 15 May 2023; accepted 31 July 2023; published online 30 September 2023

Abstract Radiation is the direct energy source of the surface natural environment and the main driving force of climate change. It has increasingly become an important meteorological factor affecting the surface heat exchange and glacier mass balance, especially in the glacier changes of the Greenland Ice Sheet (GrIS). Due to the harsh climatic conditions of GrIS and sparse observed data, it has become an important way to obtain radiation data from reanalysis datasets. However, the applicability of these radiation data on GrIS is uncertain and worth exploring. In this work, we evaluate five reanalysis datasets (the fifth generation of European Centre for Medium-Range Weather Forecasts (ERA5), European Centre for Medium-Range Weather Forecasts Interim Reanalysis (ERA-Interim), Japanese 55-year Reanalysis (JRA55), National Centers for Environmental Prediction Reanalysis II (NCEP2) and Modern-Era Retrospective analysis for Research and Applications, Version 2 (MERRA-2)) during 1997–2022 using observations from 26 Program for Monitoring the Greenland Ice Sheet (PROMICE) automatic weather stations (AWSs) and 3 K-transect AWSs on GrIS. The conclusions are as follows: ERA5 has the best performances in downward shortwave radiation (SWD) as well as downward and upward longwave radiation (LWD and LWU), but the performance is not the best in upward shortwave radiation (SWU). Based on the radiation budget analysis with ERA5 during 1979–2022, the fluctuation of longwave radiation is greater than that of shortwave radiation. The seasonal variation of shortwave radiation is obvious, while that of longwave radiation is small. The increasing trend of longwave radiation may result from global warming, in which ice sheets absorb more solar radiation and the surface heats up significantly, emitting more LWU.

Keywords **Greenland Ice Sheet**, **downward shortwave radiation**, **upward shortwave radiation, downward longwave radiation**, **upward longwave radiation, reanalysis datasets**, **automatic weather stations**

Citation: Che J H, Huai B J, Sun W J, et al. Performance of surface radiation products of Greenland Ice Sheet using in-situ measurements. Adv Polar Sci, 2023, 34(3): 190-219, doi: 10.12429/j.advps.2023.0002

1 Introduction

The Greenland Ice Sheet (GrIS) covers an area of about 1.7×10^6 km^2, with a length of about 2200 km from south to north. It is the second-largest ice sheet in the world except for Antarctica (Steffen and Box, 2001). Solar radiation is one of the most important sources of energy on the Earth's surface (Wang et al., 2021). The radiation budget affects the energy balance at the Earth's surface, and

* Corresponding author, E-mail: 616070@sdnu.edu.cn

also affects the melting and disintegration of the ice sheet. Therefore, it is particularly important to study the radiation flux and its change for the prediction of future melting changes of the GrIS (Bamber and Riva, 2010).

The sum of longwave and shortwave radiation determines the energy budget of the earth-atmosphere system and greatly control the local climate (Power and Mills, 2005). There are automatic weather stations (AWSs) observing radiation flux on the GrIS, but they are few in number and mostly located in coastal areas due to the harsh climate in the region, which makes equipment maintenance difficult. As a result, there are many missing values in the observed data and we cannot obtain the long-term radiation datasets of the entire Greenland surface (Fausto et al., 2012). Remote sensing and reanalysis datasets make up for this defect (Trenberth and Guillemot, 1998). Remote sensing mainly obtains observation data through satellites and simulates surface radiation by using the physical model of atmospheric radiation transmission (Schroeder et al., 2009; Zhang et al., 2015), which has the advantage of high spatial resolution, but its time coverage is limited (Liang et al., 2006). Moreover, due to the complex characteristics of remote sensing data, the accuracy of radiation products may be affected (Peng, 2019). In the 1990s, reanalysis datasets emerged to avoid this time series of shortcomings by optimally combining observations from different types and sources with short-term weather forecasts through a data assimilation system, which has the advantages of continuous time series, easy access and coverage of the entire Greenland surface (Trenberth and Olson, 1988). Thus it has played an increasing role in estimating radiation changes in various regions of the global (Bengtsson et al., 2007; Zhao et al., 2010). Due to the reanalysis datasets are assimilated by different data and means, the global performance capacity of each reanalysis dataset is also different, which will also make the analysis related to radiation quantity show great uncertainty and error (Wang and Dickinson, 2013). Therefore, it is necessary to evaluate the performance of each reanalysis dataset, so that the reanalysis datasets with better performance in different regions can be selected for further study. Radiation is the most important energy input for ice sheet surface melt, and the change of radiation will directly affect the amount and area of melt. The study of radiation is of great significance to the surface melt of the GrIS.

At present, previous studies have evaluated the radiation data of reanalysis (Griggs and Bamber, 2008; Cox et al., 2014; Lenaerts et al., 2017; Seo et al., 2020). Although some reanalysis radiation datasets have been evaluated on GrIS, they use less measured data and lack comparison between multiple datasets. For example, Cox et al. (2014) analyzed the downward longwave radiation (LWD) over GrIS using surface-based observations from Summit Station on GrIS and European Centre for Medium-Range Weather Forecasts Interim Reanalysis (ERA-Interim) LWD fields. The results showed that ERA-Interim performed reasonably well at Summit Station in simulating of LWD. However, other radiation components were not studied and comparison with other reanalysis data was not made. In evaluating cloud cover characteristics using Greenland satellite datasets and three reanalysis products ((NCEP1), the second NCEP-Department of Energy (DOE) Atmospheric Model Intercomparison Project (NCEP2), and ERA-40), Griggs and Bamber (2008) found that the reanalysis datasets were inconsistent in modeling radiation. This result suggests that different reanalyses may be inaccurate in estimating radiation balance over the GrIS. More research has focused on the Arctic rather than GrIS. For example, Seo et al. (2020) assessed net surface radiation over the Arctic using data from the fifth generation of European Centre for Medium-Range Weather Forecasts (ERA5), National Centre for Environmental Prediction (NCEP), Cloud and Earth Radiant Energy System (CERES) Energy Balanced and Filled (EBAF), and Global Energy and Water Exchanges (GEWEX). They found that ERA5 had the highest accuracy. Lenaerts et al. (2017) compared the downward radiation of the multi-reanalysis combined with CMIP5 and found significant but inconsistent deviations in the downward radiation component. Huang et al. (2017) used five reanalysis datasets in Arctic region (70°N–90°N) to compare surface longwave and shortwave radiation fluxes derived from NASA CERES-MODIS (CM). All reanalysis showed positive deviations from the northern and eastern coasts of Greenland. Both these studies all contribute to understand the accuracy of radiation products at high latitudes and the differences between products, but they do not focus on reanalyses over the GrIS. Serreze et al. (1998) found the NCEP-NCAR products capture 50%–60% of the observed spatial variance in global radiation during most months. At present, there are few assessments of radiative products on the GrIS, and there is a lack of systematic and complete assessment of radiative products from reanalysis data. Therefore, this work uses the data of 29 AWSs in the Programme for Monitoring of the Greenland Ice Sheet (PROMICE) and K-transect on GrIS from 1997 to 2022 and five reanalysis datasets (ERA5, ERA-Interim, JRA55, NCEP2, MERRA-2) are evaluated and analyzed for their applicability.

The organization of this paper is as follows: The data used in this study (observational data and five reanalysis datasets) are presented in section 2; The sections 3.1 and 3.2 introduce the assessment results and the radiation budget analysis based on ERA5 (1979–2022), and section 3.3 is the discussion part. Finally, a summary is given.

2 Data and methods

2.1 In-situ observations

We used daily downward shortwave radiation (SWD), upward shortwave radiation (SWU), downward longwave radiation (LWD) and upward longwave radiation (LWU) data from 26 AWSs in the PROMICE network (Fausto et al.,

2021). These data are operated by the Geological Survey of Denmark and Greenland (GEUS) in collaboration with the National Space Research Institute of the Technical University of Denmark (Ahlstrøm and Team, 2008). We used data from three AWSs along the K-transect in southwest GrIS, i.e., three Institute for Marine and Atmospheric research Utrecht (IMAU) AWSs (S5, S6, S9). The K-transect was established by the Greenland Ice Margin Experiment (GIMEX) (Oerlemans and Vugts, 1993; Kuipers Munneke et al., 2018).

The distribution of AWSs in Greenland is shown in Figure 1a and the topography is shown in Figure 1b. The locations, elevations and observation periods of these stations are shown in Table S1.

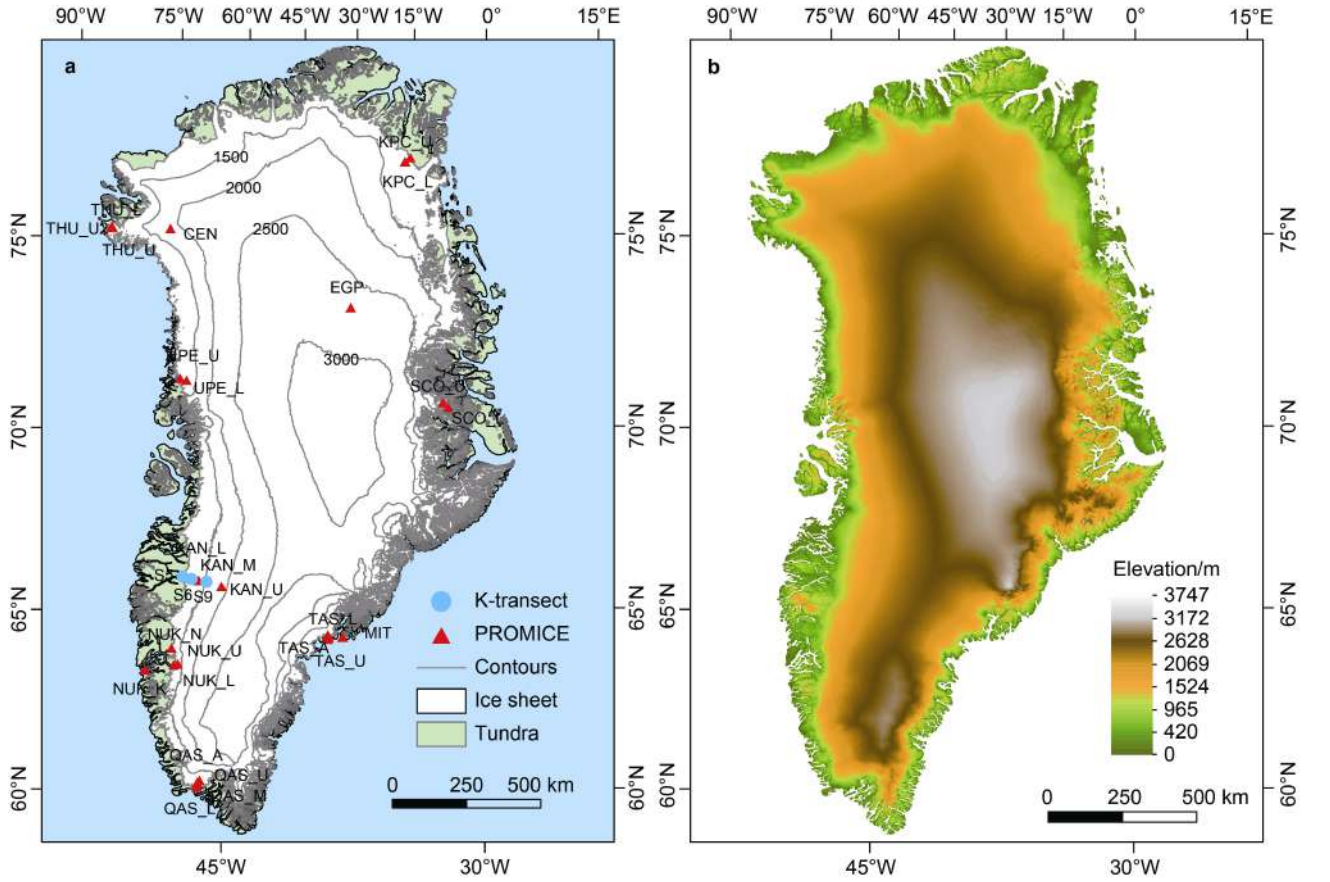

Figure 1 **a**, Location map of the research area and AWSs used in this study: The blue circle represents the AWSs of the K-transect, and the red triangle represents the PROMICE AWSs; **b**, Topographic map of Greenland.

2.2 Reanalysis products

2.2.1 ERA5

The ERA5 reanalysis is the fifth generation of global atmospheric reanalysis from the European Centre for Medium-Range Weather Forecast (ECMWF), covering the period from 1940 to the present. It provides hourly data on SWD, LWD, SWN (net shortwave radiation) and LWN (net longwave radiation) from which we can calculate SWU and LWU. The ERA5 has a temporal resolution of 1 h and a spatial resolution of 0.25°×0.25°. Assimilation schemes for ERA5 reanalysis are 10 mixed 4-Dimensional Variational Analysis (4D-Var) methods, Ensemble of Data Assimilation technology, the latest version of the high-resolution Integrated Forecast System (IFS), Earth System Models and observation data assimilation system CY41r2 Global Spectral Model. There are 137 mixed sigma-pressure (mode) levels in the vertical direction, the resolution of which is T639 (~31 km) in the horizontal direction and T319 (~63 km) in the vertical direction. The vertical direction is the highest level from class 137 to 0.01 hPa (80 km) (Hoffmann et al., 2019; Hersbach et al., 2020).

2.2.2 ERA-Interim

The ERA-Interim reanalysis is sponsored by the European Union and run by the ECMWF. The dataset adopts 4D-Var method, IFS and Cy31r2 Global Spectral Model, combined with improved humidity analysis, satellite data error correction and other technologies. Moreover, the horizontal resolution is improved to T255 (~79 km) (Berrisford et al., 2011; Dee et al., 2011). In this paper, 12-hour grid data with a spatial resolution of 0.125°×0.125° is obtained from the ECMWF. The data includes SWD, LWD, SWN and LWN, from which we calculated SWU and LWU. And the time range was January 1997 to August 2019.

2.2.3 JRA55

JRA55 was jointly launched by the Japan Meteorological Agency (JMA) and the Central Research Institute of Electric Power Industry (CRIEPI). JRA55 uses a more advanced 4D-Var method to provide data from January 1958 to the present (Ebita et al., 2011; Kobayashi et al., 2015). Many deficiencies of JRA-25 have been well corrected in the JRA55 version, such as upgrading the spatial resolution grid from T106L40 to TL319L60. In short, compared with JRA25, JRA55 reanalysis data is more complete (Kobayashi et al., 2015; Peng, 2019). In this work, we use SWD, SWU, LWD and LWU data with 3 h, 0.56°×0.56° resolution.

2.2.4 MERRA-2

MERRA-2 is a high-resolution global reanalysis product developed by Global Modeling and Assimilation Office (GMAO) in the National Aeronautics and Space Administration (NASA). It aims to produce a regularly gridded, uniform global atmospheric record, covering the era of satellite observations from 1980 to the present. To achieve this goal, MERRA-2 updates the analysis protocols and models of the Goddard Earth Observation System (GEOS), using version 5.12.4 of the GMAO/GEO-5 data assimilation system. The spatial resolution of MERRA-2 is 0.5°×0.625° (Gelaro et al., 2017). We use the data of SWD, LWD, LWU, and SWN of MERRA-2, and calculate SWU through SWN and SWD.

2.2.5 NCEP2 (NCEP-DOE)

NCEP2 (NCEP-DOE) reanalysis is a global reanalysis from 1979 to the present, with a time resolution of the day (Kistler et al., 2001). The NCEP2 reanalysis project was established to provide an improved version of the original NCEP-NCAR reanalysis (Kalnay et al., 1996; Kanamitsu et al., 2002). The NCEP2 model has the same resolution as the T62 Gaussian grid (2.5°×2.5°) with 28 vertical sigma levels in the NEP-NCAR reanalysis project. NCEP2 is a "second generation" reanalysis, which uses an improved assimilation procedure based on 4D-Var with greater emphasis on accuracy, resolution, and long-term trends. Chou and Lee (1996) replaced the parameterization method of Lacis and Hansen (1974) and alleviated the overestimation of surface solar radiation in NCEP-NCAR (Saha et al., 2010). Here we use SWD, SWU, LWD and LWU data. The information for all the reanalyses is shown in Table 1.

Table 1 Summary of information of the five reanalyses used in this study

Name	Organization	Country or region	Temporal resolution	Spatial resolution	Period
ERA5	ECMWF	Europe	1 h	0.25°×0.25°	1997-01–2022-12
ERA-Interim	ECMWF	Europe	12 h	0.125°×0.125°	1997-01–2019-08
JRA55	JMA	Japan	3 h	0.56°×0.56°	1997-01–2022-12
MERRA-2	NASA/GMAO	United States	1 h	0.5°×0.625°	1997-01–2022-12
NCEP2	NCEP	United States	24 h	2.5°×2.5°	1997-01–2022-12

2.3 Methods

For PROMICE observational data, monthly shortwave and longwave radiation were calculated only when valid daily data were more than or equal to 90% available. Seasonal and annual data were not calculated when monthly data were missing (Zhang et al., 2022). For the K-transect observed hourly data, daily data can be calculated only when the effective hourly data is greater than or equal to 90% available, and the other data is the same as PROMICE.

We used bilinear interpolation method to extract SWD, SWU, LWD and LWU data of corresponding AWSs, and carried out comparative analysis. Then three classical statistical indicators were used to evaluate the performance of the five reanalyses, that is correlation coefficient (R), root mean square error (RMSE), and bias (BIAS).

By calculating the values of three evaluation indicators R, RMSE and BIAS between the reanalysis data and the measured data, rank scoring (R_s) was performed as the objective function, and a score of 0–10 was assigned according to the differences in the performance of the five reanalyses. The formula is as follows:

$$R_s = \mathrm{Int}\left(\frac{x_i - x_{\min}}{x_{\max} - x_{\min}} \times 10\right), \quad (1)$$

x_i is the relative error between the statistical eigenvalues of the reanalyzed data and the measured data, and $x_{\max}$ and $x_{\min}$ are the maximum and minimum values of the error, respectively. First, the R_s of different evaluation indicators is calculated for each set of reanalysis data, and the final score is obtained by the average of the corresponding scores of all evaluation indicators. The smaller the score, the better the applicability of reanalysis data. However, the R_s value cannot represent the actual simulation accuracy of specific reanalysis data, and is currently mostly used in the applicability evaluation of atmospheric circulation models in various regions (Li et al., 2011; Liu et al., 2011, 2013).

3 Results and discussions

3.1 Performance of the reanalysis datasets

3.1.1 Daily scale performance

Figure 2 shows the performance of daily radiation components from five reanalyses based on observations. All reanalyses could present SWD change (R>0.94, p<0.05), suggesting they could reflect long-term SWD change well. However, MERRA-2 and NCEP2 have higher BIAS relative to AWSs. MERRA-2 systematically underestimates SWD, but NECP2 overestimates SWD below 350 W·m^{-2} due to more SWD outputs in most seasons except June, July and August (JJA). Compared to ERA-Interim, ERA5 has not improved the performance of SWU and even become

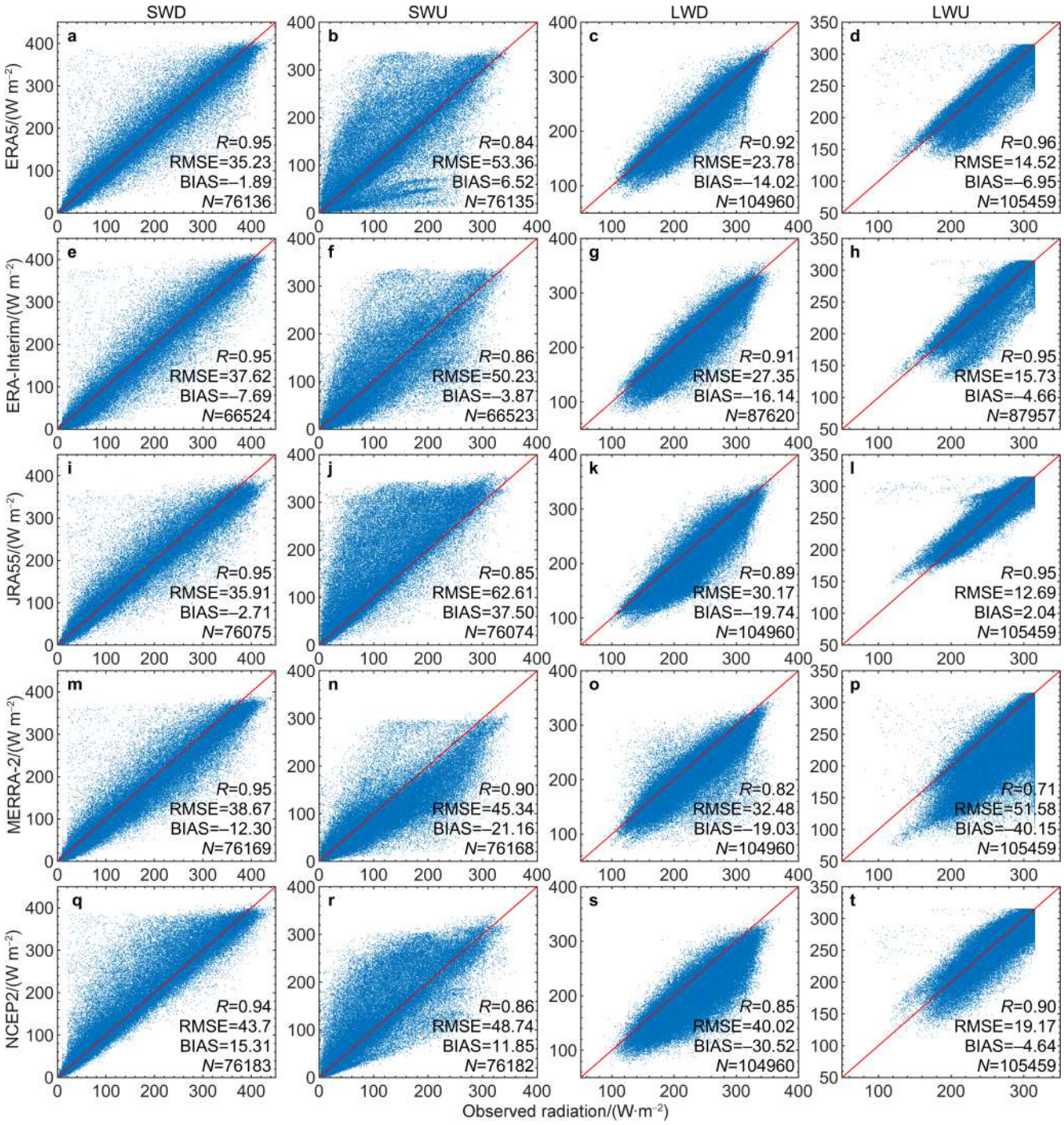

Figure 2 Comparison of daily observed SWD, SWU, LWD, LWU with 5 reanalysis datasets. **a**–**d**, Observed and ERA5 SWD, SWU, LWD and LWU, respectively ; **e**–**h**, Same as **a**–**d** but for ERA-Interim; **i**–**l**, Same as **a**–**d** but for JRA55; **m**–**p**, Same as **a**–**d** but for MERRA-2; **q**–**t**, Same as **a**–**d** but for NCEP2.

more terrible. JRA55 overestimates SWU in all seasons and the high RMSE (62.61 W·m^{-2}) shows it hardly presents SWU conditions over the GrIS. Compared with other reanalyses, ERA-Interim still is a good SWU product in the GrIS. Besides, all reanalyses underestimate LWD over the GrIS, with systematically negative BIAS occurring in all reanalyses. However, their correlation with observations still performs well (R>0.82, p<0.05), suggesting that reanalyses could be used for simulating LWD anomalies change. In fact, the underestimation of LWD results from reanalyses underestimating LWU over the GrIS except JRA55. Given the BIAS difference between LWD and LWU in JRA55 and NCEP2, there may be potential problems for the cloud radiation parameterization scheme in these two reanalyses (Yeo et al., 2022). In addition, MERRA-2 performs worst for LWU, it underestimates greatly summer LWU conditions. Overall, reanalyses could simulate SWD well over the GrIS and all reanalyses could present daily radiation change well with high correlation values, especially ERA5. R_s sequencing results of four radiation components of five reanalyses are shown in Figure 3a.

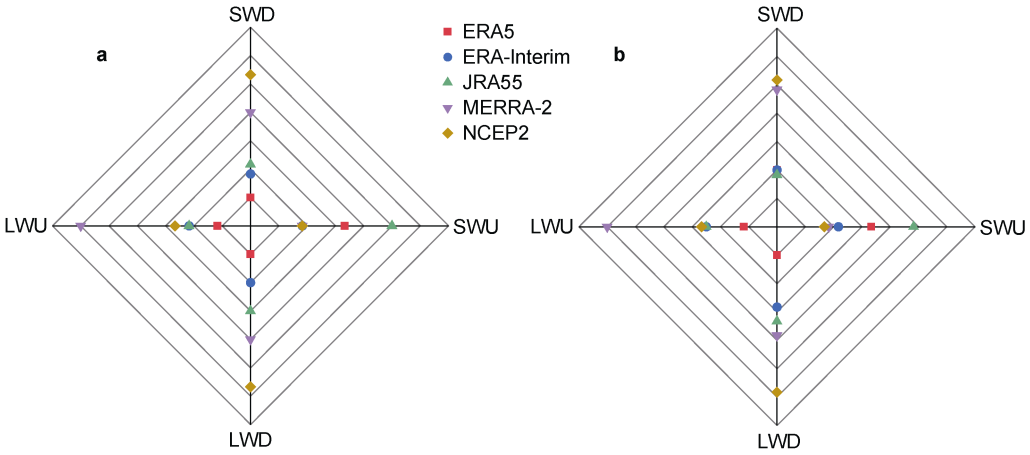

Figure 3 R_s score results of five reanalyses radiation four components at daily (**a**) and monthly (**b**).

A comprehensive analysis of the four radiation components shows that ERA5 has a good performance in radiation simulation. To further look into the performance of ERA5 at each AWS, we analyze the R, RMSE and BIAS of SWD in detail (Figure 4). SWD of ERA5 at different stations and regions shows great differences and has a high R-value in each station (R>0.86, p<0.05). RMSE ranges from 20 to 55 W·m^{-2}. Among the magnified 27 AWSs, 16 AWSs are underestimated and 11 stations are overestimated. Among them, 3 AWSs in THU-transect (Figure 4d) and 2 AWSs in UPE-transect (Figure 4g) all underestimate SWD. Both AWSs in the SCO-transect (Figure 4v) overestimate SWD. The RMSE and BIAS of THU_U2 are relatively large, which may be caused by the effect of elevation, there is a big difference between the station location of THU_U2 and the elevation of adjacent cells (Minola et al., 2020; Molina et al., 2021). It is also possible that the actual received SWD is different from the SWD flux simulated by ERA5 due to the topography (Gao and Hao, 2014; Longo-Minnolo et al., 2022; Vanella et al., 2022).

The three indicators (R, RMSE, BIAS) of SWU, LWD and LWU of ERA5 are respectively shown in Supplementary Figure S1, Figure S2, Figure S3. The three indicators (R, RMSE, BIAS) of SWD, SWU, LWD and LWU of ERA-Interim, JRA55, MERRA-2 and NCEP2 are shown in Supplementary Table S2, Table S3, Table S4 and Table S5, respectively. The simulation of ERA5 is better for LWD, but all the stations show negative deviation.

3.1.2 Monthly scale performance

Figure 5 shows the performance of monthly radiation components from five reanalyses based on observations, respectively. All reanalyses could present SWD change (R>0.99, p<0.05), and have extremely high R-values, suggesting they reflect long-term SWD change well. However, ERA-Interim, MERRA-2 and NCEP2 have higher BIAS relative to AWSs. MERRA-2 systematically underestimates SWD, but NECP2 overestimates SWD. This is the same as the daily data as the monthly data is averaged from the daily data. Compared to ERA-Interim, ERA5 has not significantly improved the performance of SWU, and the difference of performance between them is small. JRA55 overestimates SWU in all seasons and the high RMSE (50.52 W·m^{-2}) indicating that it has little ability to simulate SWU on GrIS. This may be due to the fact that the parameterization scheme of JRA55's snow ice albedo is fixed, and the change of snow ice albedo is instantaneous (Dorman and Sellers, 1989; Kobayashi et al., 2015). Compared with other reanalyses, ERA5 and ERA-Interim still are good SWU products in the GrIS. Compared to daily data, ERA5 has improved the simulation performance of SWU in monthly data. Besides, all reanalyses underestimate LWD over the GrIS, with systematically negative BIAS

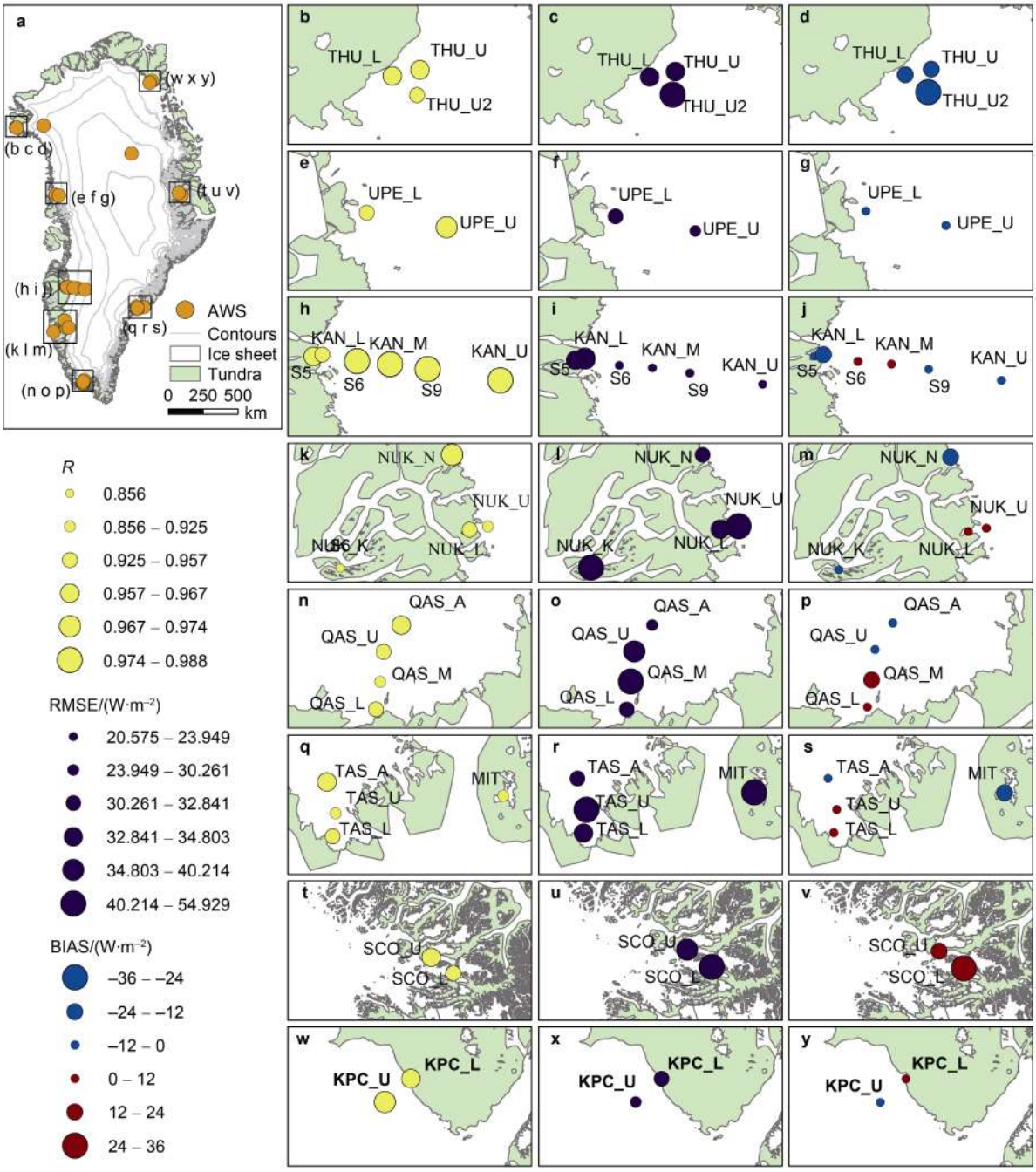

Figure 4 Spatial distribution of *R* (yellow), RMSE (purple) and BIAS (blue or red) of SWD at daily scale ERA5. All AWSs are located on the GrIS (**a**). THU-transect (**b**–**d**); UPE-transect (**e**–**g**); KAN-transect (**h**–**j**); NUK-transect (**k**–**m**); QAS-transect (**n**–**p**); TAS-transect (**q**–**s**); SCO-transect (**t**–**v**); KPC-transect (**w**–**y**).

occurring in all reanalyses. However, their correlation with observations still performs well (R>0.89, p<0.05), suggesting that reanalyses could be used for simulating LWD anomalies change. In fact, with the exception of JRA55, the negative deviation of LWD is due to the underestimation of LWU on GrIS. Given the BIAS difference between LWD and LWU in JRA55, there may be potential problems for the cloud radiation parameterization scheme in the reanalyses (Yeo et al., 2022). In addition, MERRA-2 performs worst for LWU, it underestimates summer LWU conditions by about 40 W·m^{-2}. Overall, reanalyses simulate SWD and LWD well over the GrIS and all reanalyses could present monthly radiation change well with high correlation values, especially ERA5. R_s sequencing results of four radiation components of five reanalyses are shown in Figure 3b.

A comprehensive analysis of the four radiation components shows that ERA5 has a good performance in

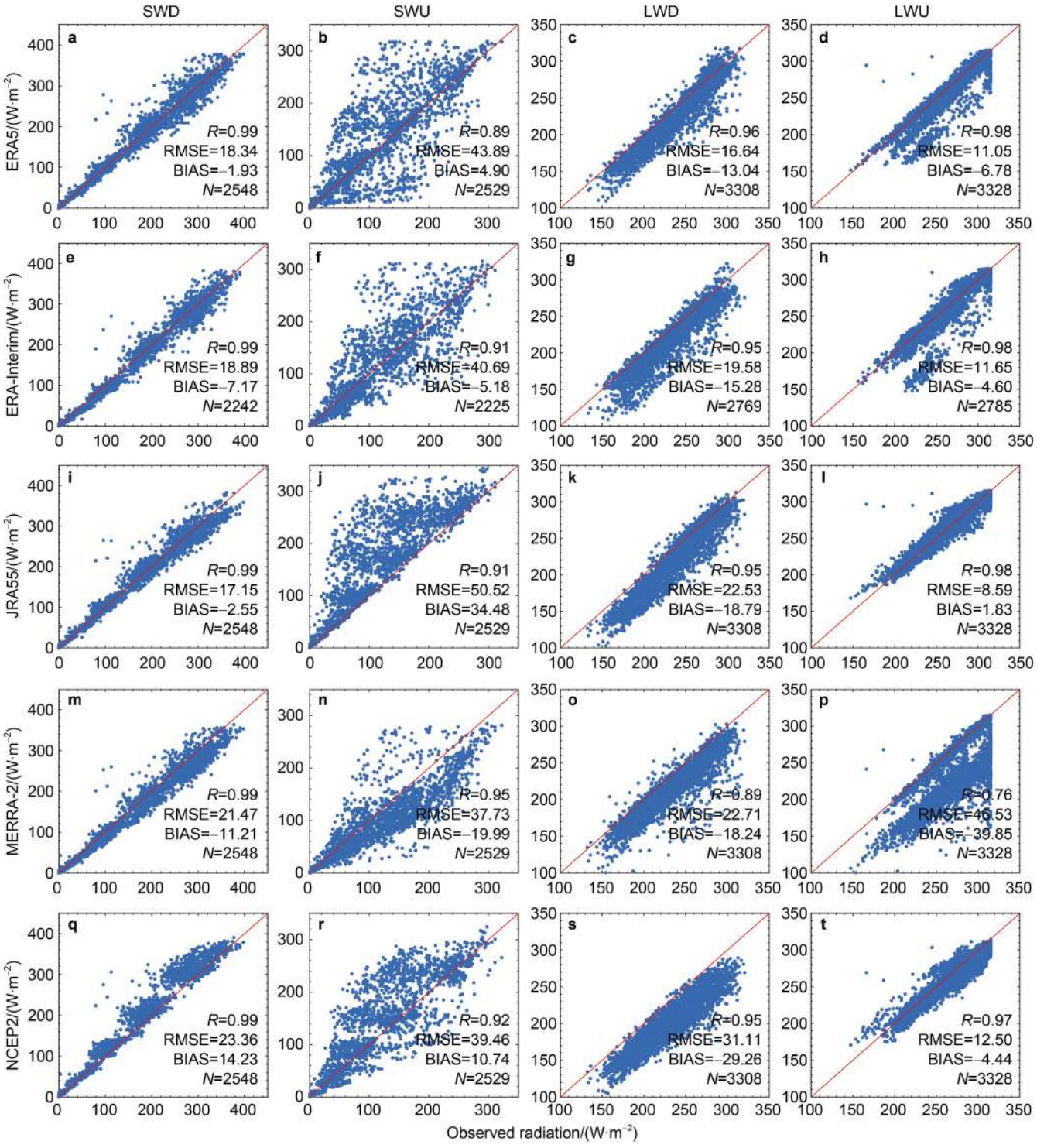

Figure 5 Comparison of monthly observed SWD, SWU, LWD, LWU with 5 reanalysis datasets. **a**, Observed and ERA5 SWD; **b**, Observed and ERA5 SWU; **c**, Observed and ERA5 LWD; **d**, Observed and ERA5 LWU; **e**–**h**, Same as **a**–**d** but for ERA-Interim; **i**–**l**, Same as **a**–**d** but for JRA55; **m**–**p**, Same as **a**–**d** but for MERRA-2; **q**–**t**, Same as **a**–**d** but for NCEP2.

radiation simulation. To further look into the performance of ERA5 at each AWS, we analyze the *R*, RMSE and BIAS of LWD in detail (Figure 6). The spatial distribution of *R*, RMSE and BIAS of LWD of ERA5 is significantly different. RMSE ranges from 8.50 to 43.07 W·m^{-2}. The *R* of KAN_M station is the highest (*R*=0.99), and that of TAS_A is the worst. All AWSs show negative BIAS, indicating that ERA5 significantly underestimates LWD. Among them, SCO_L (Figure 6v) severely underestimates LWD, and in the daily data, the same problem exists for the two AWSs in

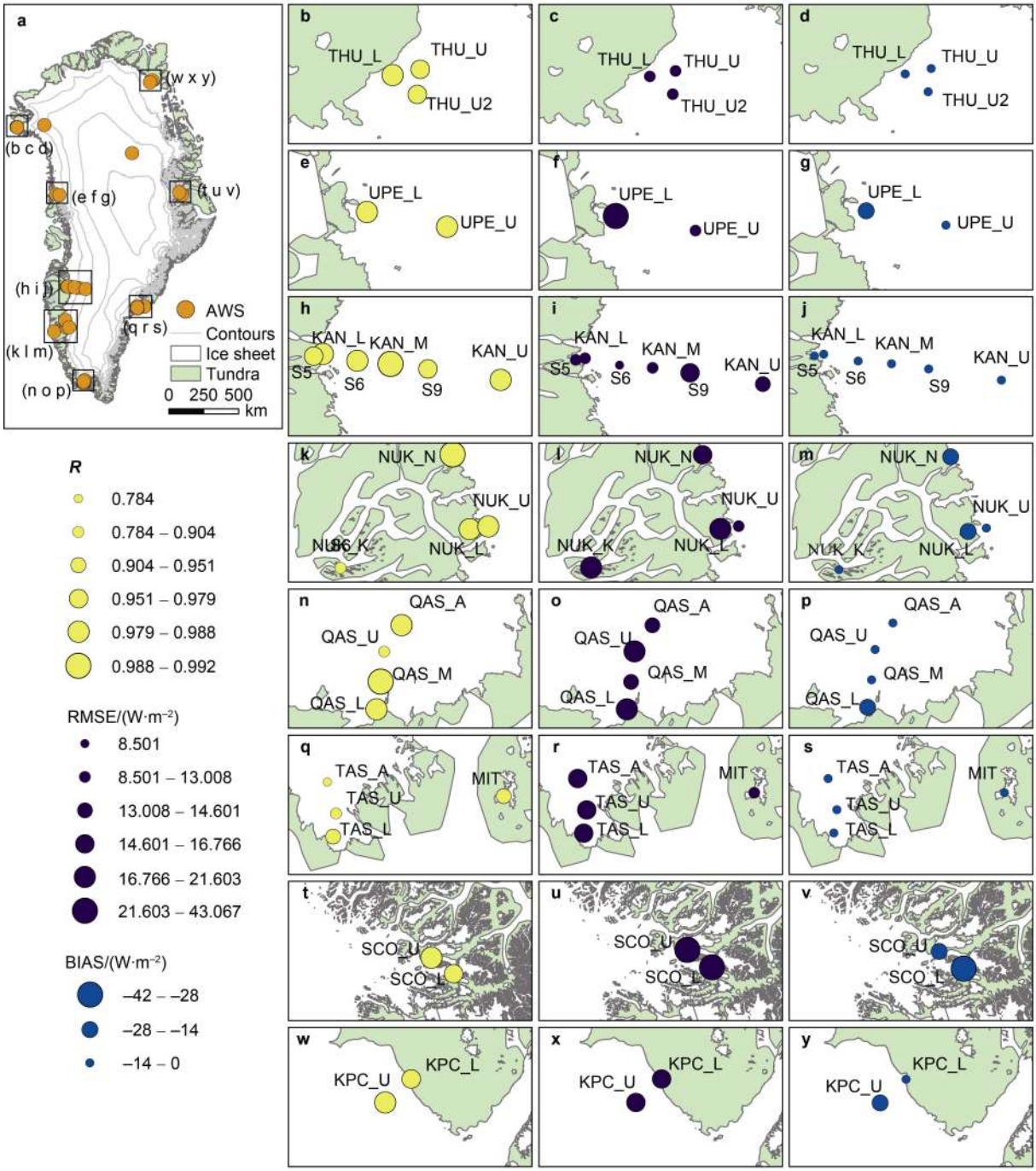

Figure 6 Spatial distribution of *R* (yellow), RMSE (purple) and BIAS (blue) of LWD at monthly scale ERA5. All AWSs are located on the GrIS (**a**); THU-transect (**b**–**d**); UPE-transect (**e**–**g**); KAN-transect (**h**–**j**); NUK-transect (**k**–**m**); QAS-transect (**n**–**p**); TAS-transect (**q**–**s**); SCO-transect (**t**–**v**); KPC-transect (**w**–**y**).

the SCO-transect (Figure S2v).

The *R*, RMSE and BIAS of SWD, SWU and LWU of ERA5 are shown in Figure S4, Figure S5, Figure S6. The *R*, RMSE and BIAS of SWD, SWU, LWD and LWU at the other four reanalysis datasets are shown in Table S6, Table S7, Table S8, Table S9. The simulation of ERA5 on the AWSs is also that SWD is better than SWU, and there is underestimation in most AWSs of LWU.

By analyzing the seasonal cycle of three evaluation indexes (*R*, RMSE and BIAS) with these reanalyses in different radiation component in Figure 7, the following conclusions can be drawn. For SWD, ERA5 has a higher *R* in each month than the other four reanalysis datasets (ERA-Interim, JRA55, MERRA-2, NCEP2). JRA55's *R* decreases significantly in March and ERA-Interim's *R* decreases significantly in November. The simulation

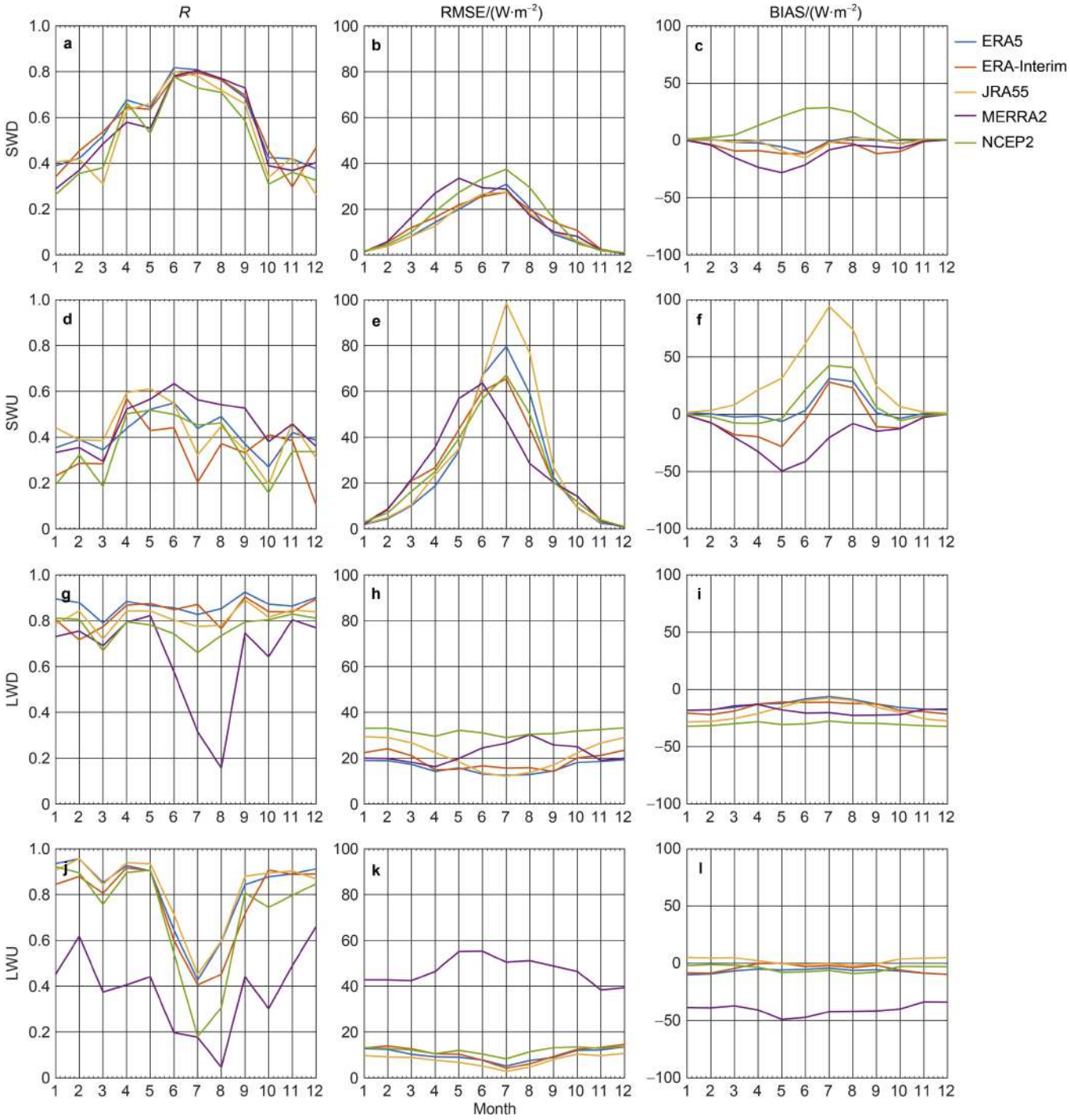

Figure 7 Monthly changes of *R*, RMSE and BIAS of SWD of five reanalysis datasets (ERA5, ERA-Interim, JRA55, MERRA-2, NCEP2). **a**, *R* of observed and five reanalysis datasets for SWD; **b**, RMSE of observed and five reanalysis datasets for SWD; **c**, BIAS of observed and five reanalysis datasets for SWD; **d**–**f**, Same as **a**–**c** but for SWU; **g**–**I**, Same as **a**–**c** but for LWD; **j**–**l**, Same as **a**–**c** but for LWU.

performance of five reanalysis datasets are higher in summer than in other seasons. When comparing RMSE, NCEP2 and MERRA-2 are higher than the other three reanalysis datasets (ERA5, ERA-Interim, JRA55) with a large deviation. In all reanalysis datasets, RMSE is largest in summer and smallest in winter, which is because SWD is basically absent in winter and SWD is large in summer. Compared with SWD, the simulation performance of SWU decreases significantly. The values of RMSE and BIAS are large and there are obvious seasonal fluctuations, with the worst performance in summer and the best performance in winter. ERA-Interim and JRA55 perform worse than the

other three reanalysis datasets. For LWD, there is a significant decrease in *R* of MERRA-2 in summer, and the simulation performance is poor. Four reanalysis datasets have no seasonal fluctuations in RMSE and BIAS, and the change is little. ERA5 performs better than the other four reanalysis datasets. RMSE and BIAS do not have seasonal fluctuations, which is the same for LWU and LWD. However, the RMSE and BIAS of MERRA-2 is significantly higher than those of the other four reanalysis datasets, and the *R* is significantly lower, indicating its poor ability to simulate LWU on GrIS. The poor performance of longwave radiation may be caused by the problem of parametric scheme (Yeo et al., 2022). The *R* values of the five reanalysis datasets have significant seasonal fluctuations in simulating LWU, with poor performance in summer and better performance in winter.

3.2 Radiation budget of Greenland during 1979–2022

Through the evaluation of the four components of radiation (SWD, SWU, LWD, LWU) of five reanalysis datasets, ERA5 is relatively a good reanalysis product. Therefore, this work analyzes the four components of seasonal and annual radiation in Greenland from 1979 to 2022 by using the data of ERA5 (Rossow and Dueñas, 2004; Pinker et al., 2005).

The intensity of shortwave radiation is affected by solar elevation angle, cloud cover, aerosol and water vapor (Gu et al., 2001; Pfister et al., 2003), and the main source of the SWD is solar radiation. The time series of summer anomaly shows that the summer shortwave radiation flux has a downward trend since 2000, and the annual variation is mainly affected by the summer radiation flux, which also has a downward trend (Figure 8). There is no shortwave radiation in winter, so the anomaly time series fluctuation is minimal. However, longwave radiation shows an upward trend at seasonal and annual scales. The interannual fluctuation of longwave radiation may be greatly affected by summer, and less affected by other seasons. In winter, the time series fluctuates the most and the annual longwave radiation flux fluctuates the most smoothly. The anomaly time series fluctuation of longwave radiation is larger than that of shortwave radiation. The increasing trend of longwave radiation is explained in detail in the spatial distribution of the trend below.

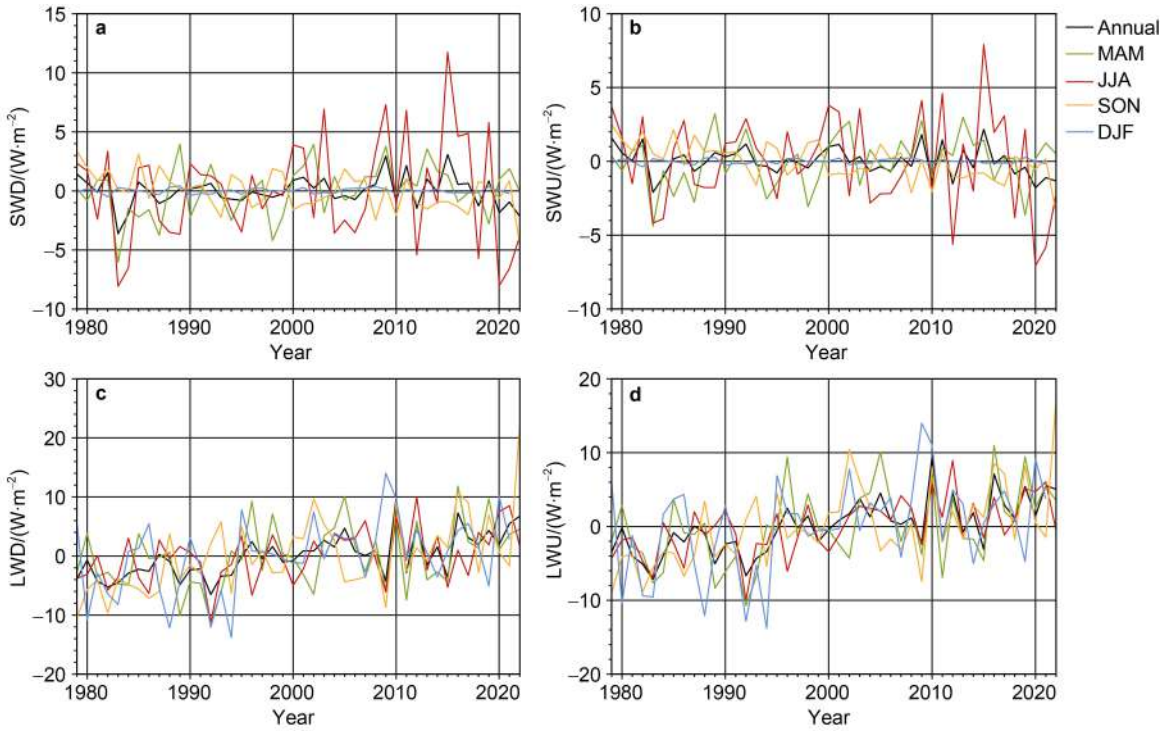

Figure 8 The four radiation components relative to the multi-year average time series of radiation anomalies from 1979–2022. **a**, SWD; **b**, SWU; **c**, LWD; **d**, LWU. MAM indicates March, April, May; JJA indicates June, July, August; SON indicates September, October, Novermber; DJF indicates December, January, February.

The shortwave radiation flux is lower than longwave radiation flux. The main source of shortwave radiation is solar radiation, while the longwave radiation can come from the radiation emitted by the surface, atmospheric radiation, etc. The main reason for the low shortwave radiation flux is that there is no shortwave radiation in winter, so the average annual radiation value is low. The average annual radiation flux of shortwave radiation is concentrated in 80–160 $W \cdot m^{-2}$ (Figure 9), and the radiation flux in the south is larger than that in the north, showing the latitude zonality. SWU is

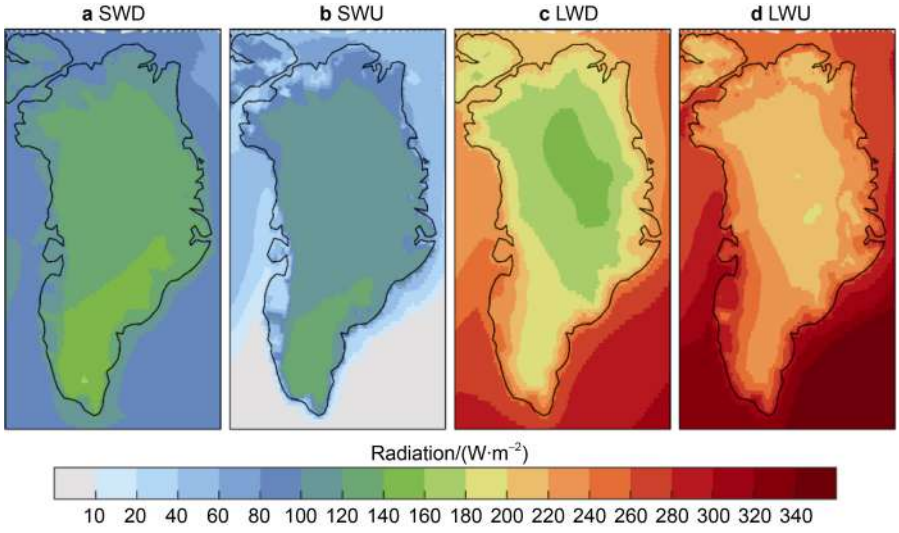

Figure 9 Multi-year average radiation from 1979 to 2022. **a**, SWD; **b**, SWU; **c**, LWD; **d**, LWU.

mainly affected by SWD, so the multi-year average of SWU is lower than that of SWD. The average annual radiation flux of longwave radiation is greater than 140 W·m^{-2}. LWD is mainly affected by LWU, so LWD flux is lower than LWU flux. Shortwave radiation and longwave radiation present different situations at the edge of the GrIS and the coastal areas of Greenland. Shortwave radiation has a low radiation flux in the coastal areas, while longwave radiation has a high radiation flux in the coastal areas. This is mainly influenced by the underlying surface, such as the underlying surface of the ice sheet, tundra, ocean and sea ice, and therefore the albedo is different. The low albedo in the southern coastal areas leads to the obvious low SWU flux. The longwave radiation absorbs more heat and has a larger longwave radiation flux.

Because Greenland has polar nights in winter, shortwave radiation is almost zero in winter. In spring and autumn, due to the influence of solar elevation angle, the shortwave radiation flux is small, and there is significant latitude zonality (Figure 10). The ice sheet receives more solar radiation in summer than in other seasons. SWD fluxes are greater on the ice sheet than in coastal areas. We speculate that the main reason is cloud cover (Abe et al., 2016; Kim et al., 2020; Li and Xu, 2020). On GrIS, there is less evaporation and less cloud cover. Therefore, clouds have little shading effect on solar radiation, and most solar radiation directly reaches the surface, forming a large radiation flux. On the other hand, the coastal area of Greenland has high evaporation, high cloud cover and strong shading, and the solar radiation reaching the surface will be significantly reduced. Therefore, the SWD flux in the seas around Greenland is smaller than that of GrIS. The obvious difference of SWD in the east and west of Greenland Ice Sheet in summer may be due to the influence of Greenland blocking index (GBI). When GBI intensifies, there is less cloud cover and more SWD. When the GBI intensity of western Greenland and eastern Greenland is different, the SWD of eastern and western Greenland is different (Lewis et al., 2021; Preece et al., 2022). Longwave radiation is not affected by the solar elevation angle, there is no the latitude zonality. Overall, the radiation flux within the ice sheet is lower than in the coastal area, which may be mainly influenced by the (underlying surface) albedo. Summer radiation flux is greater than other seasons.

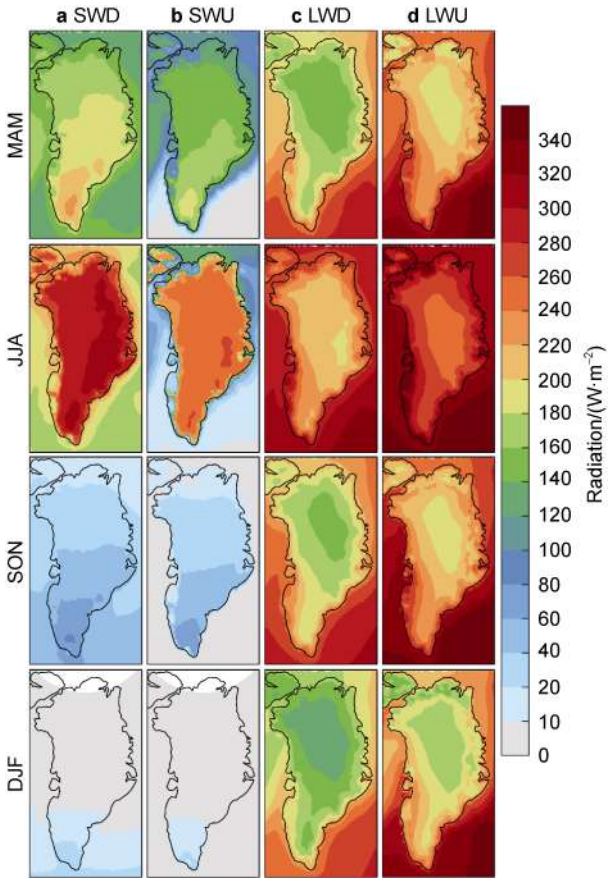

Figure 10 Multi-year average seasonal radiation from 1979 to 2022. **a**, SWD; **b**, SWU; **c**, LWD; **d**, LWU.

For the GrIS, the trend of shortwave radiation is not significant, varying in the range of −0.4–0.4 $W \cdot m^{-2} \cdot (10\ a)^{-1}$, while the trend of longwave radiation is obviously rising in the range of 0.8–2.0 $W \cdot m^{-2} \cdot (10\ a)^{-1}$ (Figure 11). The variation trend in the interior of the ice sheet is not obvious, but the radiation in the coastal areas of Greenland have a large variation. SWU has a decreasing trend in the eastern and northwestern coastal areas of Greenland, probably due to global warming, melting of sea ice and lower albedo. The increasing trend in longwave radiation may be result from global warming, in which ice sheets absorb more solar radiation and the surface heats up significantly, emitting more LWU. There is an anomaly in northwest Greenland that is significantly different from other regions. The reason may be that the sea ice concentration areas have a higher albedo than other regions, which leads to an increasing trend of SWU and a decreasing trend of longwave radiation (Renfrew et al., 2021).

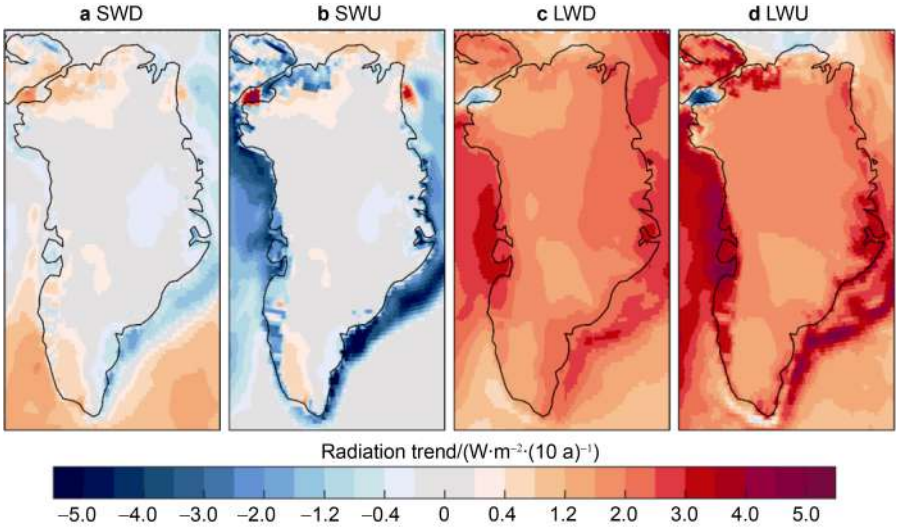

Figure 11 Radiation change trend from 1979 to 2022. **a**, SWD; **b**, SWU; **c**, LWD; **d**, LWU.

3.3 Discussions

It is found that ERA5, ERA-Interim, JRA55, MERRA-2, and NCEP2 are all able to roughly fit SWD, SWU, LWD, and LWU. However, the simulation performance of SWU on both daily and monthly scales is relatively poor, which may be caused by inaccurate estimation of underlying surface types in reanalysis products (Wei and Li, 2003; Liang et al., 2015; Zhang et al., 2021, 2023). On the monthly scale, there is a significant underestimation in the LWD simulation, and a certain deviation in the LWU radiation simulation (Wang, 2022).

On both daily and monthly time scales, none of the reanalysis is optimal when simulating the four components of radiation (Wang, 2021). This may be caused by different boundary layer processes and observations using different models when producing reanalysis. ERA5 has better performance in radiation simulation because it uses the 4D-Var data assimilation and model prediction generation of the IFS CY41r2 (Hoffmann et al., 2019; Hersbach et al., 2020). The JRA55 adopts a 4D-Var data assimilation system and variational deviation correction of satellite radiation, and adds a new data source (Kobayashi et al., 2015). However, these optimizations do not significantly affect the SWU simulation performance, and the radiation performance of JRA55 needs to be improved. The MERRA-2 reanalysis adopts the GEOS 5.12.4 model and updates the Clintrial Integration Solution scheme to reduce some errors in the observation system (Wu et al., 2002; Rienecker et al., 2011; Gelaro et al., 2017), the simulation of longwave radiation is poor, and the simulation quality is obviously different in different months, so the simulation is relatively poor. In order to fundamentally solve the accuracy of the radiation reanalysis, further research should be carried out from the aspects of improving satellite sensors, reducing the influence of cloud cover and quantifying the influence of complex terrain on reanalysis products (Xu et al., 2020; Wang, 2021).

In addition to being affected by the assimilation system of the reanalysis, the accuracy of satellite sensors and topographic conditions, meteorological factors such as aerosol, cloud cover, water vapor, solar elevation angle also affect the solar radiation and thus affect the accuracy of the reanalysis (Wang, 2022; Wang et al., 2022). At the same time, the surface albedo is also an important factor affecting the reflectivity of solar radiation, directly affecting the SWU and LWU fluxes (Ruckstuhl et al., 2008; Zhou et al., 2013; Wang, 2021).

Cloud cover is an important factor affecting the four components of radiation, among which cloud cover will not only weaken solar radiation, but also exert various influences on solar radiation by its various physical properties, cloud cover conditions and optical properties (Gu et al., 2001; Pfister et al., 2003). Previous studies have shown that underestimation of cloud cover can lead to overestimation of solar radiation in reanalysis (Zhu, 1982;

Peng, 2019). Above, the spatial patterns of the SWD in summer presented in this work further confirmed that SWD was affected by cloud cover (Abe et al., 2016; Kim et al., 2020; Li and Xu, 2020). However, Zhang (2019) suggested that there was a small correlation between cloud cover and SWD, which might be caused by different study regions. The influence of cloud on solar radiation is very complicated. Different geometric properties such as cloud height, cloud shape and cloud thickness, as well as different physical, chemical and optical properties of cloud will have different effects on solar radiation (Shen et al., 2008). Thus, although changes in total cloud cover currently observed are difficult to fully explain changes in ground-based solar radiation, the important effect of changes in cloud on solar radiation cannot be denied (Shen et al., 2008). In addition, clouds cannot directly affect LWU, but they can affect surface temperature and thus LWU by influencing SWD. Aerosols are another important and complex influence factors on solar radiation, either directly reflecting, scattering or absorbing solar radiation, or indirectly by altering the microphysical properties of clouds (Shen et al., 2008). At the same time, the influence of different aerosols on solar radiation also varies greatly (Shi et al., 2008). But in general, an increase (decrease) in aerosols also generally reduces (increases) the amount of solar radiation reaching the surface. In the last 50 years, there have been two major eruptions with global impacts: The eruptions of Mount El Chichón (Mexico 1982) and Mount Pinatubo (Philippines 1991) significantly increased the natural aerosol concentration and optical thickness on a global scale (Mishchenko et al., 2007), which significantly weakened the direct radiation reaching the ground and enhanced the scattered radiation (Robock, 2000). The apparent low value of shortwave radiation in 1983 may be related to the 1982 eruption (Figures 8a, 8b), but the 1991 eruption did not show apparent effect. Anthropogenic aerosols are mainly the aerosols emitted by burning fossil fuels in recent decades due to global industrial and economic development, such as sulfate and black carbon, which contribute about 1/3 of the global average aerosol optical thickness (Streets et al., 2006). Aerosols have a negative forcing effect on the surface shortwave radiation, which may cause the reduction of shortwave radiation.

4 Conclusions

Based on five reanalysis datasets from 29 AWSs on the GrIS, we evaluate SWD, SWU, LWD, and LWU of ERA5, ERA-Interim, JRA55, MERRA-2 and NCEP2. On the daily scale, ERA5 is superior for all radiation components except SWU. And the comprehensive analysis suggests that ERA5 should be the better choice to fill the blank regions of Greenland. The five reanalyses all show relatively poor performance of SWU. In simulating of LWD and LWU, ERA5 has the best simulation performance.

By analyzing the radiation budget during 1979–2022 with ERA5, the time series of shortwave radiation is smaller than longwave radiation. The multiyear seasonal average of shortwave radiation is mainly affected by the solar elevation angle in spring, autumn and winter, while the multiyear seasonal average of longwave radiation is mainly affected by surface albedo. The inland GrIS has high albedo and low longwave radiation flux, whereas ice sheet margins and coastal areas are the opposite. Longwave radiation has an obvious increasing trend, while shortwave radiation trend is not obvious, but there is an increasing trend in some regions.

Author contributions Che J H, Zhang Q L, Wu J K, Kang L M, Teng X R and Yang X H wrote the paper; Che J H, Zhang Q L, Wu J K, Teng X R and Huai B J analyzed the data; Huai B J, Sun W J, Ding M H, Wang L, Yan J P, Zhao S H edited the paper.

Conflicts of interest The authors declare no conflict of interest.

Data availability statement The PROMICE observations are available online (http://promice.org/download-data). ERA5 data are available online (https://cds.climate.copernicus.eu/#!/home). ERA-Interim data are available online (https://apps.ecmwf.int/datasets/data/interim-mdfa/levtype=sfc/). JRA55 data are available online (https://rda.ucar.edu/datasets/ds628.0/). MERRA-2 data are available online (https://search.earthdata.nasa.gov/search?fp=MERRA-2). NCEP2 data are available online (https://www.esrl.noaa.gov/psd/data/gridded/data.ncep.reanalysis2.html).

Acknowledgments This work was funded by the Natural Science Foundation of China (Grant no. 42171121) and the open fund of Key Laboratory of Oceanic Atmospheric Chemistry and Global Change, Ministry of Natural Resources, China (Grant no. GCMAC2206). The authors gratefully acknowledge support from data availability from PROMICE and ERA5, ERA-Interim, JRA55, MERRA-2, NCEP2. We thank Guest Editor, Dr. Tong Zhang and two anonymous reviewers for reviewing this manuscript.

References

Abe M, Nozawa T, Ogura T, et al. 2016. Effect of retreating sea ice on Arctic cloud cover in simulated recent global warming. Atmos Chem Phys, 16(22): 14343-14356, doi:10.5194/acp-16-14343-2016.

Ahlstrøm A P, Team P P. 2008. A new programme for monitoring the mass loss of the Greenland Ice Sheet. GEUS Bull, 15: 61-64, doi:10.34194/geusb.v15.5045.

Bamber J, Riva R. 2010. The sea level fingerprint of recent ice mass fluxes. Cryosphere, 4(4): 621-627, doi:10.5194/tc-4-621-2010.

Bengtsson L, Arkin P, Berrisford P, et al. 2007. The need for a dynamical climate reanalysis. Bull Am Meteorol Soc, 88(4): 495-502, doi:10.1175/bams-88-4-495.

Berrisford P, Kållberg P, Kobayashi S, et al. 2011. Atmospheric conservation properties in ERA-Interim. QJR Meteorol Soc, 137(659): 1381-1399, doi:10.1002/qj.864.

Chou M D, Lee K T. 1996. Parameterizations for the absorption of solar radiation by water vapor and ozone. J Atmos Sci, 53(8): 1203-1208,

doi:10.1175/1520-0469(1996)053<1203: pftaos>2.0.co;2.

Cox C J, Walden V P, Compo G P, et al. 2014. Downwelling longwave flux over Summit, Greenland, 2010–2012: analysis of surface-based observations and evaluation of ERA-Interim using wavelets. J Geophys Res Atmos, 119(21): 12317-12337, doi:10.1002/2014jd021975.

Dee D P, Uppala S M, Simmons A J, et al. 2011. The ERA-Interim reanalysis: configuration and performance of the data assimilation system. Q J Roy Meteor Soc, 137: 553-597, doi: 10.1002/qj.828.

Dorman J L, Sellers P J. 1989. A global climatology of albedo, roughness length and stomatal resistance for atmospheric general circulation models as represented by the simple biosphere model (SiB). J Appl Meteor, 28(9): 833-855, doi:10.1175/1520-0450(1989)028<0833: agcoar>2.0.co;2.

Ebita A, Kobayashi S, Ota Y, et al. 2011. The Japanese 55-year reanalysis "JRA-55": an interim report. Sola, 7: 149-152.

Fausto R S, van As D, Ahlstrøm A P, et al. 2012. Assessing the accuracy of Greenland Ice Sheet ice ablation measurements by pressure transducer. J Glaciol, 58(212): 1144-1150, doi:10.3189/2012jog12j075.

Fausto R S, van As D, Mankoff K D, et al. 2021. Programme for Monitoring of the Greenland Ice Sheet (PROMICE) automatic weather station data. Earth Syst Sci Data, 13(8): 3819-3845, doi:10.5194/essd-13-3819-2021.

Gao L, Hao L. 2014. Verification of ERA-Interim reanalysis data over China. J Subtrop Resour Environ, 9: 75-81.

Gelaro R, McCarty W, Suárez M J, et al. 2017. The modern-era retrospective analysis for research and applications, Version 2 (MERRA-2). J Clim, 30(13): 5419-5454, doi: 10.1175/JCLI-D-16-0758.1.

Griggs J A, Bamber J L. 2008. Assessment of cloud cover characteristics in satellite datasets and reanalysis products for Greenland. J Clim, 21(9): 1837-1849, doi:10.1175/2007jcli1570.1.

Gu L H, Fuentes J D, Garstang M, et al. 2001. Cloud modulation of surface solar irradiance at a pasture site in southern Brazil. Agric For Meteorol, 106(2): 117-129, doi:10.1016/s0168-1923(00)00209-4.

Hersbach H, Bell B, Berrisford P, et al. 2020. The ERA5 global reanalysis. QJR Meteorol Soc, 146: 1999-2049, doi:10.1002/qj.3803.

Hoffmann L, Günther G, Li D, et al. 2019. From ERA-Interim to ERA5: the considerable impact of ECMWF's next-generation reanalysis on Lagrangian transport simulations. Atmos Chem Phys, 19(5): 3097-3124, doi:10.5194/acp-19-3097-2019.

Huang Y Y, Dong X Q, Xi B K, et al. 2017. Quantifying the uncertainties of reanalyzed Arctic cloud and radiation properties using satellite surface observations. J Clim, 30(19): 8007-8029, doi:10.1175/jcli-d-16-0722.1.

Kalnay E, Kanamitsu M, Kistler R, et al. 1996. The NCEP/NCAR 40-year reanalysis project. Bull Amer Meteor Soc, 77(3): 437-471, doi:10.1175/1520-0477(1996)077<0437: tnyrp>2.0.co;2.

Kanamitsu M, Ebisuzaki W, Woollen J, et al. 2002. NCEP-DOE AMIP-II reanalysis (R-2). Bull Am Meteorol Soc, 83(11): 1631-1643, doi:10.1175/bams-83-11-1631(2002)0831631: nar>2.3.co;2.

Kim J E, Laguë M M, Pennypacker S, et al. 2020. Evaporative resistance is of equal importance as surface albedo in high-latitude surface temperatures due to cloud feedbacks. Geophys Res Lett, 47(4): e2019GL085663, doi:10.1029/2019gl085663.

Kistler R, Kalnay E, Collins W, et al. 2001. The NCEP-NCAR 50-year reanalysis: monthly means CD-ROM and documentation. Bull Amer Meteor Soc, 82(2): 247-267, doi:10.1175/1520-0477(2001)082<0247: tnnyrm>2.3.co;2.

Kobayashi S, Ota Y, Harada Y, et al. 2015. The JRA-55 reanalysis: general specifications and basic characteristics. J Meteor Soc Japan, 93(1): 5-48, doi:10.2151/jmsj.2015-001.

Kuipers Munneke P, Smeets C J P P, Reijmer C H, et al. 2018. The K-transect on the western Greenland Ice Sheet: Surface energy balance (2003–2016). Arct Antarct Alp Res, 50(1): e1420952, doi:10.1080/15230430.2017.1420952.

Lacis A A, Hansen J. 1974. A parameterization for the absorption of solar radiation in the earth's atmosphere. J Atmos Sci, 31(1): 118-133, doi:10.1175/1520-0469(1974)031<0118: apftao>2.0.co;2.

Lenaerts J T M, Van Tricht K, Lhermitte S, et al. 2017. Polar clouds and radiation in satellite observations, reanalyses, and climate models. Geophys Res Lett, 44(7): 3355-3364, doi:10.1002/2016gl072242.

Lewis G, Osterberg E, Hawley R, et al. 2021. Atmospheric blocking drives recent albedo change across the western Greenland Ice Sheet percolation zone. Geophys Res Lett, 48(10): e2021GL092814, doi:10.1029/2021gl092814.

Li F P, Xu Z X, Liu X C, et al. 2011. Assessment on performance of different general circulation models in Songhuajiang River Basin. Hydrology, 31(6): 24-31.

Li Z J, Xu K M. 2020. Arctic clouds simulated by a multiscale modeling framework and comparisons with observations and conventional GCMs. J Geophys Res Atmos, 125(1): e2019JD030522, doi:10.1029/2019jd030522.

Liang F, Bian L G, Xiao C D, et al. 2015. Evaluation of four reanalysis radiation datasets from the East Antarctic Plateau. Chin J Polar Res, 27(1): 56-64 (in Chinese with English abstract).

Liang S L, Zheng T, Liu R G, et al. 2006. Estimation of incident photosynthetically active radiation from Moderate Resolution Imaging Spectrometer data. J Geophys Res, 111(D15): D15208, doi:10.1029/2005jd006730.

Liu W F, Xu Z X, Li F P, et al. 2011. Performance of different General Circulation Models (GCMs) in the basins of southeastern China. J Subtr Resour Environ, 6: 13-23.

Liu W F, Xu Z X, Li F P. 2013. GCM preformance on simulation climatological factors in yarlung zangbo river basin basen on a ranked score method, J Beijing Normal Uni (Nat Sci), 49: 304-11.

Longo-Minnolo G, Vanella D, Consoli S, et al. 2022. Assessing the use of ERA5-Land reanalysis and spatial interpolation methods for retrieving precipitation estimates at basin scale. Atmos Res, 271: 106131, doi:10.1016/j.atmosres.2022.106131.

Minola L, Zhang F, Azorin-Molina C, et al. 2020. Near-surface mean and gust wind speeds in ERA5 across Sweden: towards an improved gust parametrization. Clim Dyn, 55(3): 887-907, doi:10.1007/s00382-020-05302-6.

Mishchenko M I, Geogdzhayev I V, Rossow W B, et al. 2007. Long-term satellite record reveals likely recent aerosol trend. Science, 315(5818): 1543, doi:10.1126/science.1136709.

Molina M O, Gutiérrez C, Sánchez E. 2021. Comparison of ERA5 surface wind speed climatologies over Europe with observations from the HadISD dataset. Int J Climatol, 41(10): 4864-4878, doi:10.1002/joc.7103.

Oerlemans J, Vugts H F. 1993. A meteorological experiment in the melting zone of the Greenland Ice Sheet. Bull Amer Meteor Soc, 74(3): 355-365, doi:10.1175/1520-0477(1993)074<0355: ameitm>2.0.co;2.

Peng X M. 2019. Error and impact factor analysis of global solar radiation reanalysis products. Master thesis, Nanjing: Nanjing University (in Chinese with English abstract).

Pfister G, McKenzie R L, Liley J B, et al. 2003. Cloud coverage based on all-sky imaging and its impact on surface solar irradiance. J Appl Meteor, 42(10): 1421-1434, doi:10.1175/1520-0450(2003)042<1421: ccboai>2.0.co;2.

Pinker R T, Zhang B, Dutton E G. 2005. Do satellites detect trends in surface solar radiation? Science, 308(5723): 850-854, doi:10.1126/science.1103159.

Power H C, Mills D M. 2005. Solar radiation climate change over southern Africa and an assessment of the radiative impact of volcanic eruptions. Int J Climatol, 25(3): 295-318, doi:10.1002/joc.1134.

Preece J R, Wachowicz L J, Mote T L, et al. 2022. Summer Greenland blocking diversity and its impact on the surface mass balance of the Greenland Ice Sheet. JGR Atmospheres, 127(4): e2021JD035489, doi:10.1029/2021jd035489.

Renfrew I A, Barrell C, Elvidge A D, et al. 2021. An evaluation of surface meteorology and fluxes over the Iceland and Greenland Seas in ERA5 reanalysis: the impact of sea ice distribution. QJR Meteoro Soc, 147(734): 691-712, doi:10.1002/qj.3941.

Rienecker M M, Suarez M J, Gelaro R. 2011. MERRA: NASA's modern-era retrospective analysis for research and applications, J Clim, 24: 3624-3648, doi: 10.1175/JCLI-D-11-00015.1.

Robock A. 2000. Volcanic eruptions and climate. Rev Geophys, 38(2): 191-219, doi:10.1029/1998rg000054.

Rossow W, Dueñas E. 2004. The international satellite cloud climatology project (ISCCP) web site: an online resource for research. Bull Am Meteorol Soc, 85: 167-172, doi:10.1175/BAMS-85-2-167.

Ruckstuhl C, Philipona R, Behrens K, et al. 2008. Aerosol and cloud effects on solar brightening and the recent rapid warming. Geophys Res Lett, 35(12): L12708, doi:10.1029/2008gl034228.

Saha S, Moorthi S, Pan H L, et al. 2010. The NCEP climate forecast system reanalysis. Bull Am Meteorol Soc, 91: 1015-1058, doi: 10.1175/2010BAMS3001.1.

Schroeder T A, Hember R, Coops N C, et al. 2009. Validation of solar radiation surfaces from MODIS and reanalysis data over topographically complex terrain. J Appl Meteorol Climatol, 48(12): 2441-2458, doi:10.1175/2009jamc2152.1.

Seo M, Kim H C, Lee K S, et al. 2020. Characteristics of the reanalysis and satellite-based surface net radiation data in the Arctic. J Sens, 2020: 1-13, 8825870doi:10.1155/2020/8825870.

Serreze M C, Key J R, Box J E, et al. 1998. A new monthly climatology of global radiation for the Arctic and comparisons with NCEP-NCAR reanalysis and ISCCP-C2 fields. J Climate, 11(2): 121-136, doi:10.1175/1520-0442(1998)011<0121: anmcog>2.0.co;2.

Shen Y B, Zhao Z C, Shi G Y. 2008. The progress in variation of surface solar rediation, factors and probable climate effects. Adv Earth Sci, 23(9): 915-924, doi: 10.11867/j.issn.1001-8166.2008.09.0915.

Shi G Y, Wang B, Zhang H, et al. 2008. The radiative and climate effects of the atmospheric aerosols. Chin J Atmos Sci, 32(4): 826-840, doi: 10.3878/j.issn.1006-9895.2008.04.11.

Steffen K, Box J. 2001. Surface climatology of the Greenland Ice Sheet: Greenland climate network 1995–1999. J Geophys Res, 106(D24): 33951-33964, doi:10.1029/2001jd900161.

Streets D G, Wu Y, Chin M. 2006. Two-decadal aerosol trends as a likely explanation of the global dimming/brightening transition. Geophys Res Lett, 33(15): L15806, doi:10.1029/2006gl026471.

Trenberth K E, Guillemot C J. 1998. Evaluation of the atmospheric moisture and hydrological cycle in the NCEP/NCAR reanalyses. Clim Dyn, 14(3): 213-231, doi:10.1007/s003820050219.

Trenberth K E, Olson J G. 1988. An evaluation and intercomparison of global analyses from the national meteorological center and the European centre for medium range weather forecasts. Bull Amer Meteor Soc, 69(9): 1047-1057, doi:10.1175/1520-0477(1988)069<1047: aeaiog>2.0.co;2.

Vanella D, Longo-Minnolo G, Belfiore O R, et al. 2022. Comparing the use of ERA5 reanalysis dataset and ground-based agrometeorological data under different climates and topography in Italy, J Hydrol: Regional Studies, 42: 101182, doi: 10.1016/j.ejrh.2022.101182.

Wang J Y. 2021. Characteristics of climate change in the Qilian Mountains over the last 40 years and the large-scale circulation. Master thesis, Jinan: Shandong Normal University (in Chinese with English abstract).

Wang K C, Dickinson R E. 2013. Global atmospheric downward longwave radiation at the surface from ground-based observations, satellite retrievals, and reanalyses. Rev Geophys, 51(2): 150-185, doi:10.1002/rog.20009.

Wang Y, Zhao X S, Mamtimin A, et al. 2021. Evaluation of reanalysis datasets for solar radiation with in situ observations at a location over the Gobi region of Xinjiang, China. Remote Sens, 13(21): 4191, doi:10.3390/rs13214191.

Wang Y S. 2022. Research on the radiation balance of the Laohugou Basin in Qilian Mountains. Master thesis, Jinan: Shandong Normal University (in Chinese with English abstract).

Wang Y S, Sun W J, Wang L, et al. 2022. How do different reanalysis radiation datasets perform in west Qilian Mountains? Front Earth Sci, 10: 852054, doi:10.3389/feart.2022.852054.

Wei L, Li D L. 2003. Evaluation of NCEP/DOE surface flux data over Qinghai-Xizang Plateau. Plateau Meteor, 22(5): 478-487.

Wu W S, Purser R J, Parrish D F. 2002. Three-dimensional variational analysis with spatially inhomogeneous covariances. Mon Wea Rev, 130(12): 2905-2916, doi:10.1175/1520-0493(2002)130<2905: tdvaws>2.0.co;2.

Xu L, Chen N C, Moradkhani H, et al. 2020. Improving global monthly and daily precipitation estimation by fusing gauge observations, remote sensing, and reanalysis data sets. Water Resour Res, 56(3): e2019WR026444, doi:10.1029/2019wr026444.

Yeo H, Kim M H, Son S W, et al. 2022. Arctic cloud properties and associated radiative effects in the three newer reanalysis datasets (ERA5, MERRA-2, JRA-55): discrepancies and possible causes. Atmos Res, 270: 106080, doi:10.1016/j.atmosres.2022.106080.

Zhang Q L, Huai B J, van den Broeke M R, et al. 2022. Temporal and spatial variability in contemporary Greenland warming (1958–2020). J Clim, 35(9): 2755-2767, doi:10.1175/jcli-d-21-0313.1.

Zhang X T, Liang S L, Wild M, et al. 2015. Analysis of surface incident shortwave radiation from four satellite products. Remote Sens Environ, 165: 186-202, doi:10.1016/j.rse.2015.05.015.

Zhang W Y. 2019. Trends in surface solar radiation and evaluation of reanalysis radiation datasets from Shule River. Master thesis, Jinan: Shandong Normal University (in Chinese with English abstract).

Zhang W Y, Wang Y T, Smeets P C J P, et al. 2021. Estimating

near-surface climatology of multi-reanalyses over the Greenland Ice Sheet. Atmos Res, 259: 105676, doi:10.1016/j.atmosres.2021.105676.

Zhang W Y, Zeng J, Wang Y T, et al. 2023. Capability of multi-reanalyses to represent precipitation over the Greenland Ice Sheet. Atmos Res, 284: 106598, doi:10.1016/j.atmosres.2022.106598.

Zhao T B, Fu C B, Ke Z J, et al. 2010. Global atmosphere reanalysis datasets: current status and recent advances. Adv Earth Sci, 25(3): 241-254, doi: 10.11867/j.issn.1001-8166.2010.03.0241.

Zhou W F, Zhao B R, Li X D, et al. 2013. Variation characteristics of the radiation budget and its component in the eastern Qinghai-Xizang Plateau. Plateau Meteor, 32(2): 2327-2333.

Zhu Z H. 1982. Multi-factors calculation on the temporal and spacial distribution of solar radiation. Acta Geographica Sinica, 37(1): 27-34, doi: 10.11821/xb198201004.

Supplementary Figures and Tables

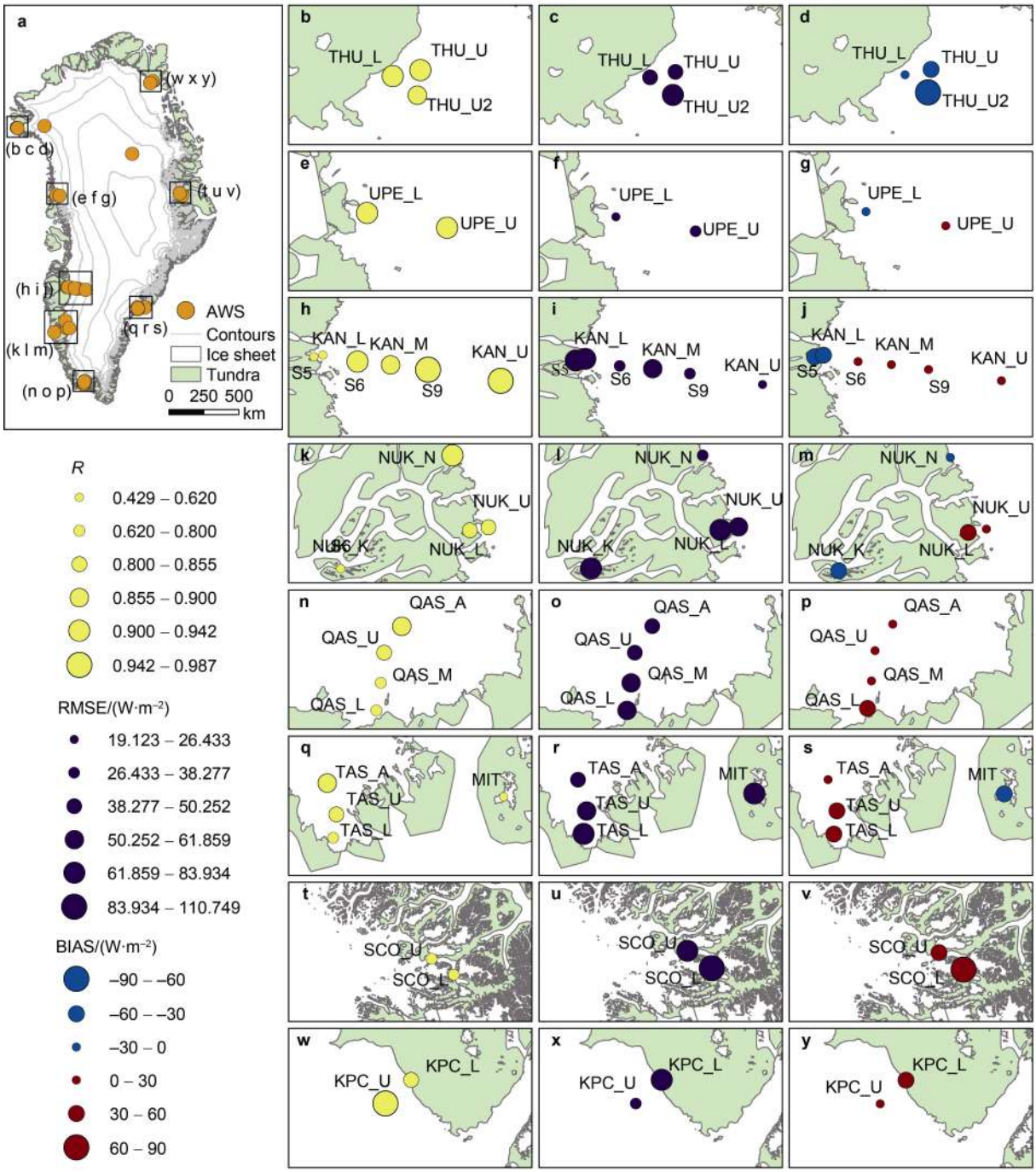

Figure S1 Spatial distribution of *R* (yellow), RMSE (purple) and BIAS (blue or red) of SWU at daily scale ERA5. All AWSs are located on the GrIS (**a**). THU-transect (**b**–**d**); UPE-transect (**e**–**g**); KAN-transect (**h**–**j**); NUK-transect (**k**–**m**); QAS-transect (**n**–**p**); TAS-transect (**q**–**s**); SCO-transect (**t**–**v**); KPC-transect (**w**–**y**).

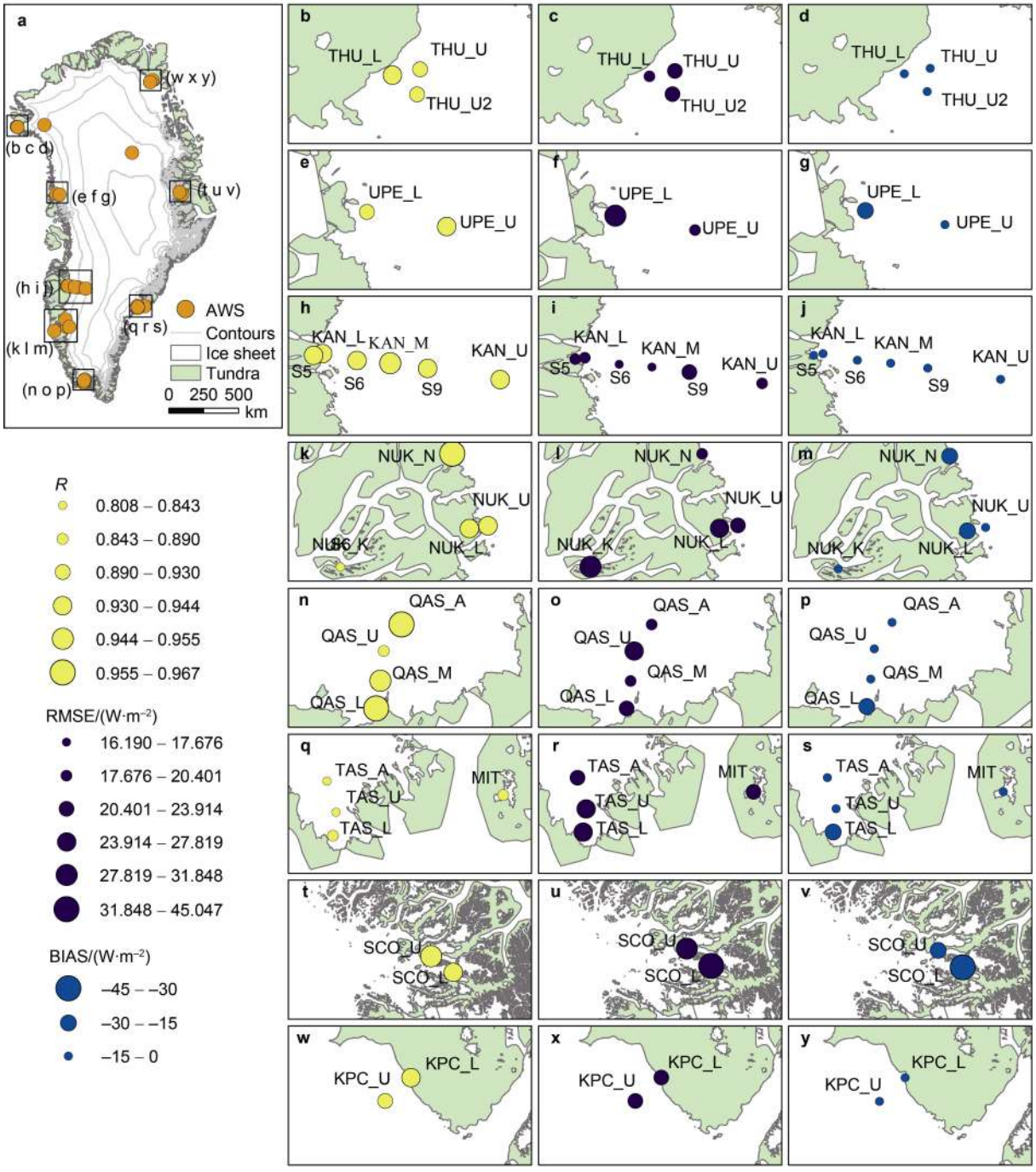

Figure S2 Spatial distribution of *R* (yellow), RMSE (purple) and BIAS (blue or red) of LWD at daily scale ERA5. All AWSs are located on the GrIS (**a**). THU-transect (**b**–**d**); UPE-transect (**e**–**g**); KAN-transect (**h**–**j**); NUK-transect (**k**–**m**); QAS-transect (**n**–**p**); TAS-transect (**q**–**s**); SCO-transect (**t**–**v**); KPC-transect (**w**–**y**).

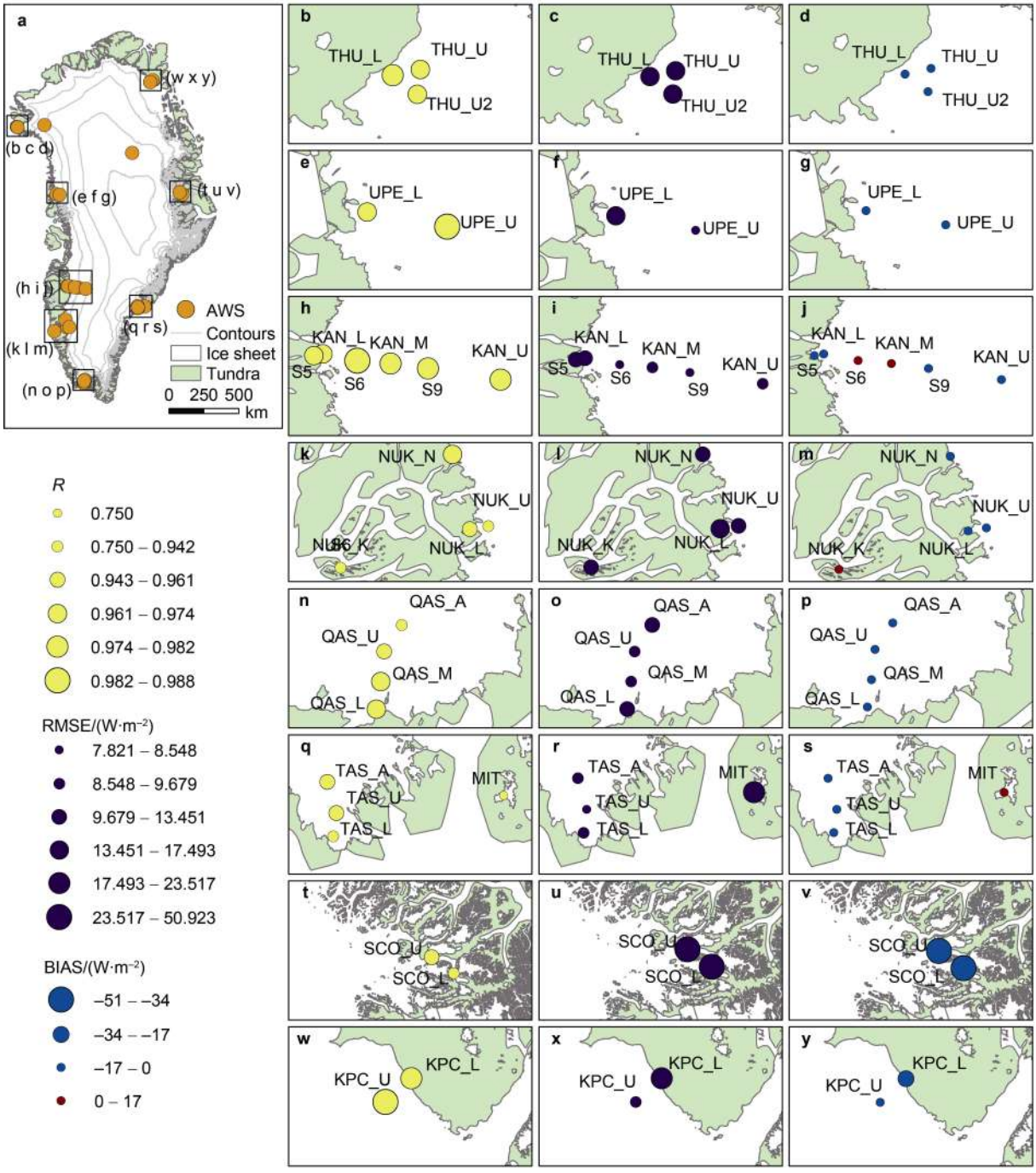

Figure S3 Spatial distribution of *R* (yellow), RMSE (purple) and BIAS (blue or red) of LWU at daily scale ERA5. All AWSs are located on the GrIS (**a**). THU-transect (**b**–**d**); UPE-transect (**e**–**g**); KAN-transect (**h**–**j**); NUK-transect (**k**–**m**); QAS-transect (**n**–**p**); TAS-transect (**q**–**s**); SCO-transect (**t**–**v**); KPC-transect (**w**–**y**).

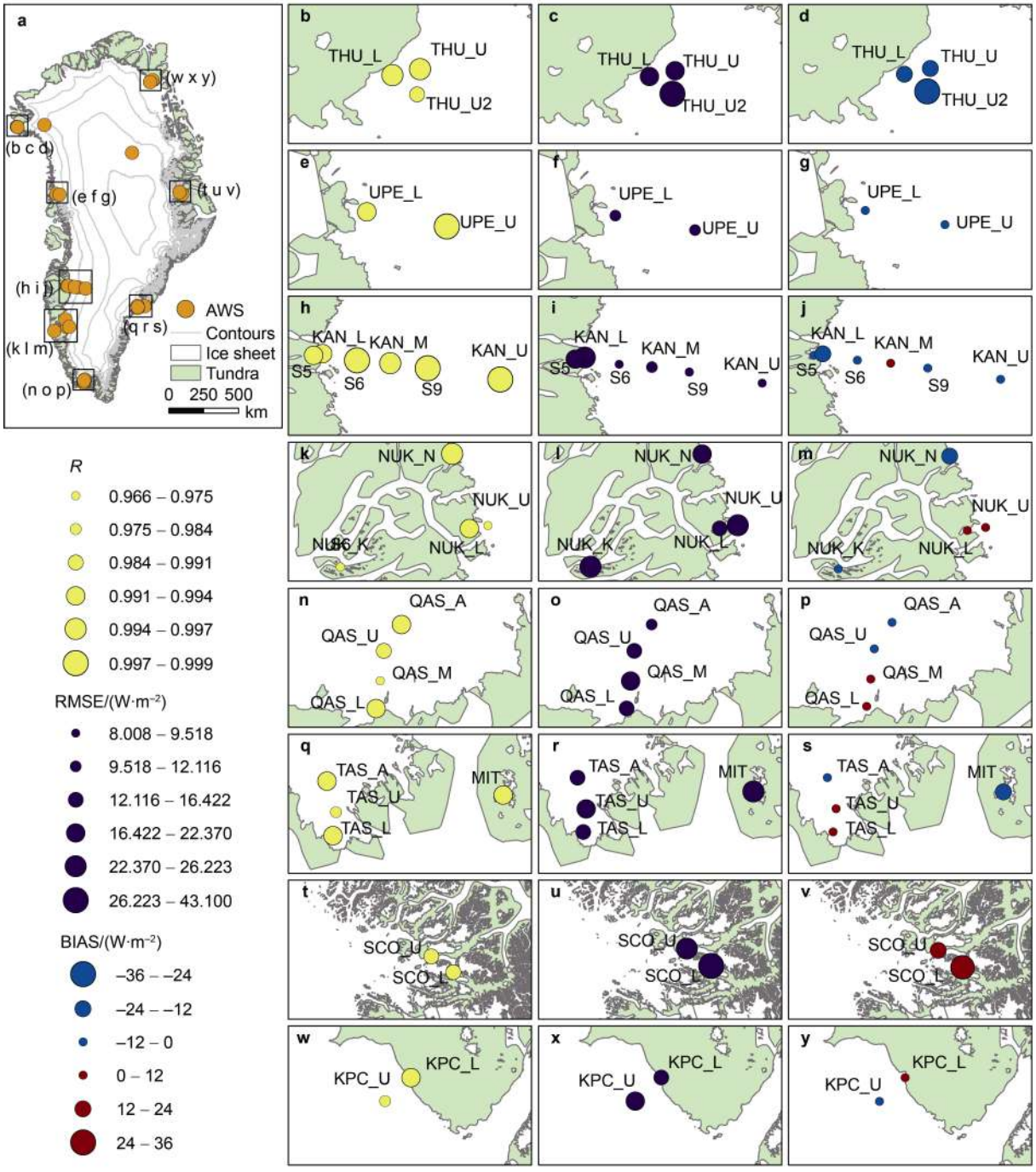

Figure S4 Spatial distribution of *R* (yellow), RMSE (purple) and BIAS (blue or red) of SWD at monthly scale ERA5. All AWSs are located on the GrIS (**a**). THU-transect (**b**–**d**); UPE-transect (**e**–**g**); KAN-transect (**h**–**j**); NUK-transect (**k**–**m**); QAS-transect (**n**–**p**); TAS-transect (**q**–**s**); SCO-transect (**t**–**v**); KPC-transect (**w**–**y**).

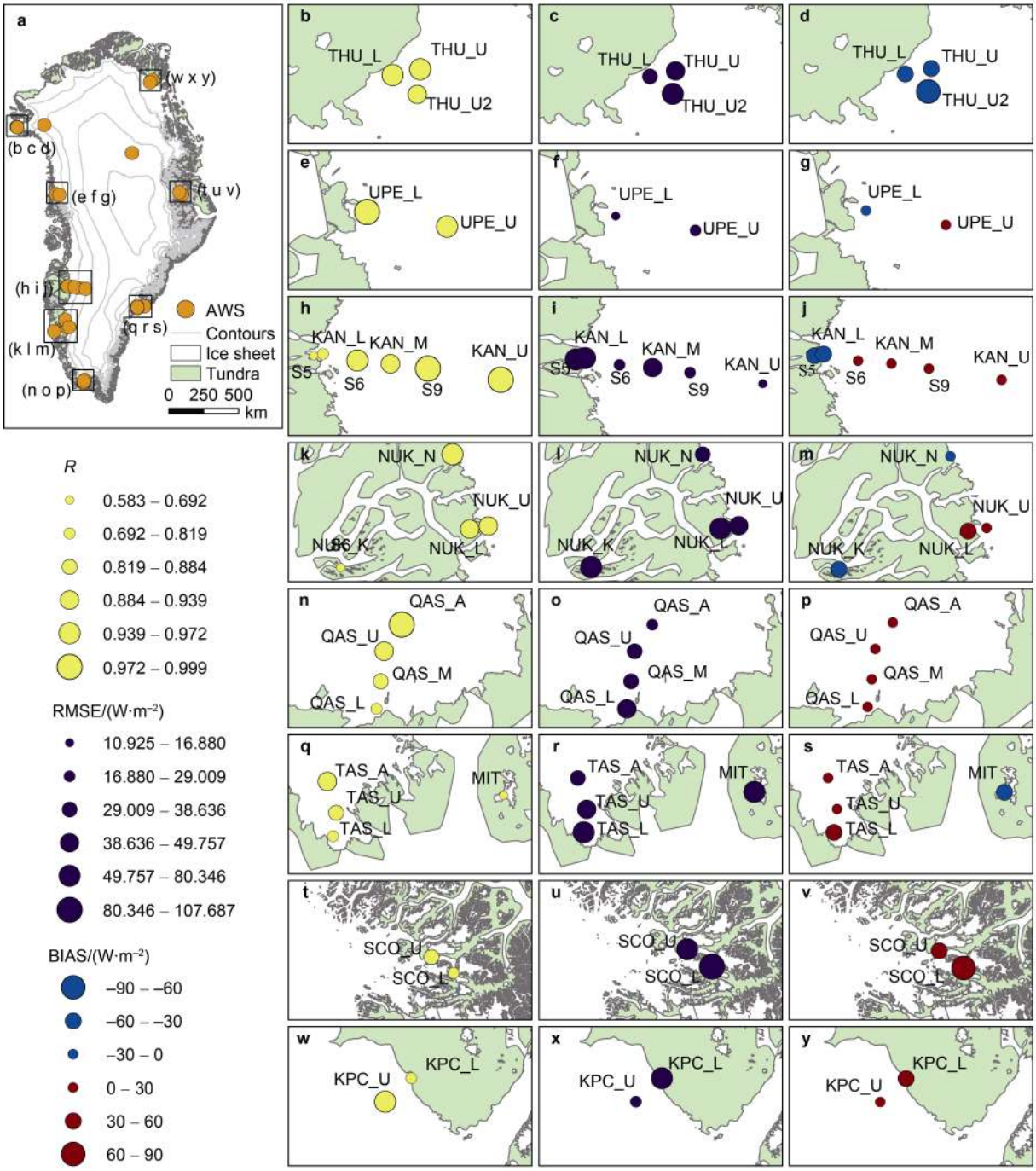

Figure S5 Spatial distribution of *R* (yellow), RMSE (purple) and BIAS (blue or red) of SWU at monthly scale ERA5. All AWSs are located on the GrIS (**a**). THU-transect (**b–d**); UPE-transect (**e–g**); KAN-transect (**h–j**); NUK-transect (**k–m**); QAS-transect (**n–p**); TAS-transect (**q–s**); SCO-transect (**t–v**); KPC-transect (**w–y**).

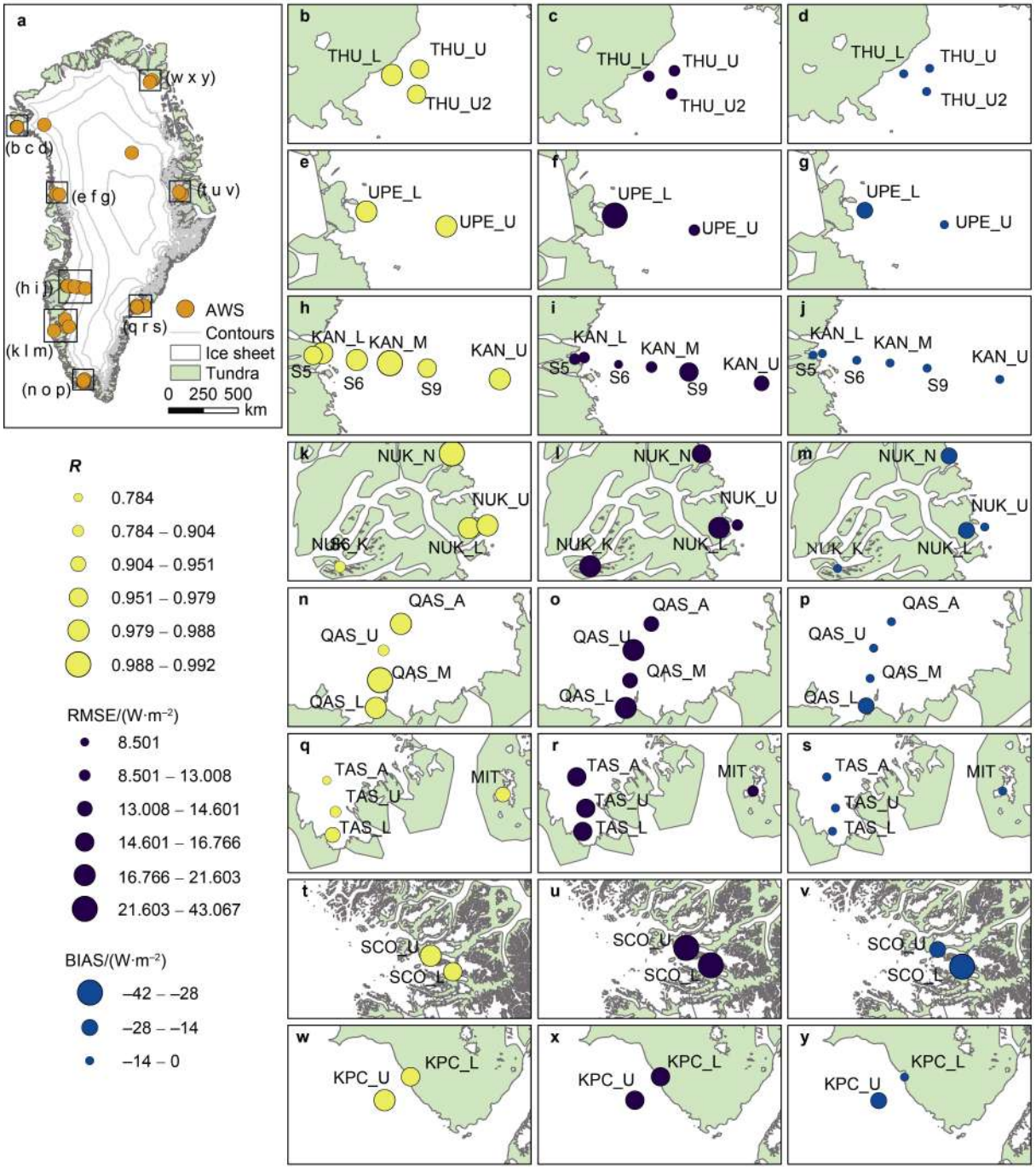

Figure S6 Spatial distribution of *R* (yellow), RMSE (purple) and BIAS (blue or red) of LWU at monthly scale ERA5. All AWSs are located on the GrIS (**a**). THU-transect (**b**–**d**); UPE-transect (**e**–**g**); KAN-transect (**h**–**j**); NUK-transect (**k**–**m**); QAS-transect (**n**–**p**); TAS-transect (**q**–**s**); SCO-transect (**t**–**v**); KPC-transect (**w**–**y**).

Table S1 Basic information of AWSs used in this study

Station name	Latitude	Longitude	Elevation/m	Data period used in this study
CEN	77.13°N	61.03°W	1884	2017-05-23–2021-08-12
EGP	75.62°N	35.97°W	2656	2016-05-01–2022-01-12
KAN_L	67.10°N	49.95°W	637	2008-09-01–2022-01-12
KAN_M	67.07°N	48.84°W	1268	2008-09-02–2022-01-12
KAN_U	67.00°N	47.03°W	1823	2009-04-04–2022-01-12
KPC_L	79.91°N	24.08°W	361	2008-07-17–2022-01-12
KPC_U	79.83°N	25.17°W	863	2008-07-17–2022-01-12
MIT	65.69°N	37.83°W	433	2009-05-04–2022-01-12
NUK_K	64.16°N	51.36°W	700	2014-07-28–2022-01-12
NUK_L	64.48°N	49.54°W	504	2007-08-20–2022-01-12
NUK_N	64.95°N	49.89°W	919	2010-07-25–2014-07-25
NUK_U	64.51°N	49.27°W	1116	2007-08-20–2022-01-12
QAS_A	61.24°N	46.73°W	1003	2012-08-20–2015-08-24
QAS_L	61.03°N	46.85°W	248	2007-08-24–2022-01-11
QAS_M	61.10°N	46.83°W	605	2016-08-11–2022-01-12
QAS_U	61.18°N	46.82°W	887	2008-08-07–2022-01-12
SCO_L	72.22°N	26.82°W	456	2008-07-22–2022-01-12
SCO_U	72.39°N	27.23°W	975	2008-07-21–2022-01-12
TAS_A	65.78°N	38.90°W	896	2013-08-28–2022-01-12
TAS_L	65.64°N	38.90°W	232	2007-08-23–2022-01-12
TAS_U	65.70°N	38.87°W	565	2008-03-11–2015-08-13
THU_L	76.40°N	68.27°W	549	2010-08-09–2022-01-12
THU_U	76.42°N	68.15°W	756	2010-08-09–2021-02-06
THU_U2	76.39°N	68.11°W	769	2018-05-22–2022-01-12
UPE_L	72.89°N	54.30°W	201	2009-08-17–2022-01-12
UPE_U	72.89°N	53.58°W	916	2009-08-18–2022-01-12
S5	67.08°N	50.10°W	490	2003-08-27–2019-09-05
S6	67.07°N	49.38°W	1020	1997-08-28–2019-09-03
S9	67.05°N	48.22°W	1520	2003-08-26–2018-08-27

Table S2 Daily data evaluation indexes of SWD for five reanalysis datasets for all stations

SWD	ERA5			ERA-Interim			JRA55			MERRA-2			NCEP2		
	R	RMSE	BIAS	*R*	RMSE	BIAS	*R*	RMSE	BIAS	*R*	RMSE	BIAS	*R*	RMSE	BIAS
CEN	0.974	30.261	−8.380	0.927	53.450	−29.723	0.970	35.558	−15.245	0.974	38.748	−22.737	0.969	31.643	−3.257
EGP	0.985	21.493	−1.394	0.979	26.448	−2.288	0.981	24.947	5.544	0.979	26.418	−9.137	0.978	27.511	7.757
KAN_L	0.950	40.210	−17.692	0.967	30.135	−5.856	0.951	37.141	−10.251	0.962	34.874	−15.054	0.936	43.830	16.010
KAN_M	0.979	23.949	0.806	0.972	30.218	−8.830	0.972	28.956	−7.696	0.972	33.436	−18.187	0.965	31.559	4.361
KAN_U	0.986	20.575	−4.869	0.976	28.753	−7.569	0.980	25.815	−7.880	0.980	30.403	−17.894	0.975	27.317	2.979
KPC_L	0.961	32.841	3.367	0.967	32.094	−2.136	0.954	38.114	−14.306	0.959	34.763	−10.146	0.942	40.065	4.226
KPC_U	0.971	28.766	−0.838	0.972	32.684	−14.234	0.969	34.285	−15.885	0.965	35.724	−16.681	0.958	34.913	1.005
MIT	0.925	47.742	−17.021	0.943	40.849	3.687	0.933	42.273	2.768	0.926	45.368	−10.428	0.901	68.023	41.672
NUK_K	0.856	54.929	−4.089	0.928	40.704	−2.220	0.884	49.861	5.969	0.852	56.504	−9.660	0.863	68.868	38.305

Continued

SWD	ERA5			ERA-Interim			JRA55			MERRA-2			NCEP2		
	R	RMSE	BIAS	*R*	RMSE	BIAS	*R*	RMSE	BIAS	*R*	RMSE	BIAS	*R*	RMSE	BIAS
NUK_L	0.954	34.803	11.559	0.949	35.324	2.369	0.940	40.375	14.792	0.937	38.249	0.991	0.887	60.532	29.529
NUK_N	0.971	32.036	−14.954	0.964	31.341	−6.556	0.962	32.204	−5.556	0.960	35.313	−14.166	0.929	46.987	18.145
NUK_U	0.922	45.871	9.362	0.911	48.025	−6.672	0.916	45.878	5.404	0.911	47.008	−6.325	0.898	53.738	16.381
QAS_A	0.966	28.987	−2.877	0.958	35.782	−15.036	0.954	35.332	−10.908	0.963	34.395	−15.994	0.961	31.097	0.862
QAS_L	0.957	32.574	7.163	0.957	33.182	0.986	0.950	33.906	2.447	0.944	36.193	−5.537	0.917	49.652	20.555
QAS_M	0.897	48.135	12.843	0.924	41.825	−1.212	0.892	46.605	5.237	0.889	47.356	0.244	0.890	52.731	19.657
QAS_U	0.938	40.214	−0.185	0.932	43.725	−10.226	0.932	42.596	−9.240	0.928	45.154	−14.935	0.938	40.510	4.638
SCO_L	0.948	52.781	35.645	0.959	44.556	24.168	0.950	44.263	26.224	0.948	40.821	18.659	0.932	54.619	34.608
SCO_U	0.960	37.711	17.177	0.967	34.096	8.285	0.962	33.032	10.334	0.960	32.208	2.006	0.946	41.271	16.879
TAS_A	0.963	31.330	−2.508	0.964	35.514	−14.325	0.963	32.622	−10.312	0.953	38.984	−18.181	0.958	36.907	15.760
TAS_L	0.955	33.608	6.472	0.955	35.273	2.499	0.952	33.900	0.507	0.945	36.675	−3.990	0.913	56.152	31.120
TAS_U	0.906	48.798	7.352	0.900	52.124	1.857	0.896	49.572	0.093	0.894	50.633	−5.118	0.887	61.774	29.391
THU_L	0.964	34.475	−16.684	0.954	42.107	−25.134	0.960	32.476	−6.025	0.960	40.050	−24.058	0.948	40.406	14.326
THU_U	0.965	34.653	−17.646	0.950	45.218	−28.741	0.964	31.712	−9.377	0.961	42.208	−28.061	0.957	35.661	11.217
UPE_L	0.956	31.599	−3.658	0.958	32.757	−2.965	0.948	35.693	8.714	0.946	35.922	−8.265	0.910	54.100	25.008
UPE_U	0.974	27.739	−6.403	0.971	31.862	−14.906	0.975	26.136	−1.820	0.971	33.523	−17.733	0.954	37.228	9.931
THU_U2	0.953	46.904	−31.163	0.919	68.095	−50.903	0.956	40.666	−21.572	0.951	55.907	−43.053	0.955	34.662	4.187
S5	0.962	33.816	−10.613	0.973	27.598	0.563	0.960	32.961	−4.881	0.969	29.866	−7.879	0.947	45.349	20.606
S6	0.980	23.877	0.148	0.974	28.952	−7.374	0.977	26.279	−3.980	0.975	31.132	−14.591	0.970	32.119	9.149
S9	0.988	20.858	−5.835	0.980	28.199	−10.412	0.982	28.133	−11.559	0.983	33.580	−20.687	0.977	28.033	−0.977

Note: Unit for both RMSE and BIAS, $W \cdot m^{-2}$.

Table S3 Daily data evaluation indexes of SWU for five reanalysis datasets for all stations

SWU	ERA5			ERA-Interim			JRA55			MERRA-2			NCEP2		
	R	RMSE	BIAS	*R*	RMSE	BIAS	*R*	RMSE	BIAS	*R*	RMSE	BIAS	*R*	RMSE	BIAS
CEN	0.968	25.803	−0.730	0.910	52.194	−30.619	0.960	29.102	4.932	0.974	33.909	−21.062	0.938	46.424	−24.129
EGP	0.987	19.123	8.360	0.981	20.095	−3.253	0.986	35.524	27.306	0.983	20.612	−9.336	0.985	24.057	14.679
KAN_L	0.620	69.868	−49.167	0.903	36.118	12.447	0.886	61.090	40.989	0.901	46.334	−33.680	0.877	64.653	44.923
KAN_M	0.873	54.837	25.858	0.857	49.985	9.928	0.871	56.557	27.468	0.925	36.905	−17.431	0.870	43.544	7.649
KAN_U	0.981	20.096	3.324	0.969	27.889	0.734	0.970	27.850	10.389	0.975	34.679	−26.151	0.978	21.296	5.819
KPC_L	0.811	76.924	50.365	0.818	67.343	31.788	0.839	69.533	46.142	0.874	44.022	14.433	0.805	71.906	45.140
KPC_U	0.952	32.786	10.990	0.933	37.220	−2.340	0.954	31.221	9.665	0.970	35.141	−26.274	0.950	30.378	5.222
MIT	0.546	82.352	−50.707	0.810	46.828	4.034	0.775	83.357	54.770	0.797	55.877	−27.975	0.785	71.973	48.224
NUK_K	0.429	75.116	−41.099	0.809	50.461	−26.702	0.799	68.418	45.733	0.668	77.005	−53.063	0.798	52.215	28.934
NUK_L	0.822	65.463	48.862	0.847	49.849	31.933	0.758	102.325	79.481	0.848	28.402	2.933	0.732	76.805	55.825
NUK_N	0.931	38.277	−22.820	0.806	51.232	12.715	0.755	79.320	48.035	0.905	50.026	−29.937	0.711	68.128	31.240
NUK_U	0.855	58.061	29.645	0.864	38.999	−4.660	0.850	63.769	36.146	0.894	42.257	−23.669	0.848	43.417	10.962
QAS_A	0.900	42.292	12.912	0.893	51.794	−34.372	0.887	45.318	14.199	0.907	49.412	−31.079	0.881	55.563	−36.062
QAS_L	0.789	53.171	32.098	0.683	45.345	−2.848	0.643	94.558	61.723	0.825	35.956	−8.599	0.739	41.389	1.063
QAS_M	0.775	52.506	20.561	0.729	52.876	−19.713	0.736	72.875	40.162	0.835	45.955	−21.067	0.754	53.222	−24.449
QAS_U	0.842	50.252	16.856	0.857	53.803	−32.467	0.820	61.141	25.873	0.867	53.370	−31.865	0.841	57.586	−35.137
SCO_L	0.752	110.749	85.779	0.737	102.875	72.412	0.764	113.359	89.311	0.814	72.020	50.737	0.808	78.816	61.515
SCO_U	0.800	83.934	57.861	0.791	77.512	44.654	0.806	88.657	63.822	0.866	48.445	23.841	0.852	55.495	35.029
TAS_A	0.894	48.106	21.415	0.909	36.446	−13.646	0.901	48.738	23.526	0.928	51.132	−37.047	0.909	49.908	−30.141

Continued

SWU	ERA5			ERA-Interim			JRA55			MERRA-2			NCEP2		
	R	RMSE	BIAS	*R*	RMSE	BIAS	*R*	RMSE	BIAS	*R*	RMSE	BIAS	*R*	RMSE	BIAS
TAS_L	0.774	65.596	40.771	0.777	50.746	18.577	0.719	87.902	59.001	0.891	32.083	−8.072	0.723	46.721	1.521
TAS_U	0.820	61.859	34.601	0.832	43.281	5.437	0.774	75.479	43.577	0.878	39.015	−19.275	0.811	42.149	−8.040
THU_L	0.927	42.035	−27.983	0.832	62.327	−42.557	0.857	63.058	39.102	0.925	48.360	−33.827	0.924	39.073	17.373
THU_U	0.923	48.657	−35.295	0.835	75.401	−57.839	0.927	42.561	22.973	0.933	60.861	−49.115	0.941	30.151	−0.194
UPE_L	0.942	26.433	−11.454	0.937	25.734	−3.347	0.907	65.855	48.503	0.939	41.151	−30.195	0.903	43.126	26.626
UPE_U	0.926	32.692	8.785	0.899	37.102	−9.260	0.899	57.489	35.084	0.948	34.352	−20.879	0.918	36.656	14.761
THU_U2	0.898	71.378	−60.416	0.775	109.857	−93.787	0.936	34.078	8.416	0.911	84.527	−75.232	0.933	36.742	−16.389
S5	0.599	70.014	−45.100	0.941	30.581	11.627	0.906	57.888	36.302	0.924	45.392	−30.802	0.925	62.745	43.153
S6	0.919	38.022	12.940	0.906	38.460	3.516	0.882	58.738	29.267	0.945	36.399	−20.120	0.905	44.129	17.522
S9	0.966	31.039	11.786	0.953	34.256	5.268	0.945	39.788	15.635	0.975	31.297	−19.954	0.965	25.280	1.002

Note: Unit for both RMSE and BIAS, $W \cdot m^{-2}$.

Table S4 Daily data evaluation indexes of LWD for five reanalysis datasets for all stations

LWD	ERA5			ERA-Interim			JRA55			MERRA-2			NCEP2		
	R	RMSE	BIAS	*R*	RMSE	BIAS	*R*	RMSE	BIAS	*R*	RMSE	BIAS	*R*	RMSE	BIAS
CEN	0.890	31.848	−22.244	0.895	31.812	−16.452	0.860	34.415	−17.932	0.726	39.926	−25.558	0.818	33.089	−16.908
EGP	0.881	29.612	−21.683	0.885	31.198	−24.060	0.872	38.789	−34.067	0.684	43.505	−32.284	0.822	42.409	−36.242
KAN_L	0.939	18.643	−6.008	0.924	25.628	−15.720	0.903	25.967	−14.143	0.862	28.710	−17.102	0.846	41.233	−32.380
KAN_M	0.950	17.676	−10.700	0.942	19.049	−9.678	0.907	24.057	−12.569	0.847	27.171	−12.899	0.837	35.085	−23.326
KAN_U	0.944	20.134	−13.763	0.928	21.659	−12.702	0.906	28.815	−20.220	0.822	30.534	−17.469	0.813	34.505	−20.663
KPC_L	0.939	21.296	−12.525	0.936	19.583	−9.448	0.902	30.118	−20.562	0.847	32.658	−18.912	0.871	35.261	−25.342
KPC_U	0.930	21.885	−14.312	0.921	17.965	−5.121	0.896	29.505	−21.001	0.847	31.536	−20.044	0.859	33.894	−24.237
MIT	0.869	22.707	−8.836	0.810	23.716	−7.988	0.835	27.124	−16.466	0.718	33.109	−16.080	0.815	56.509	−50.979
NUK_K	0.808	29.116	−1.874	0.869	28.181	−7.650	0.793	31.645	−10.987	0.705	33.598	−9.572	0.754	41.361	−27.643
NUK_L	0.939	27.819	−22.145	0.911	27.098	−18.713	0.900	36.413	−28.823	0.836	37.899	−27.252	0.842	45.149	−36.385
NUK_N	0.967	20.401	−15.500	0.955	16.566	−8.580	0.934	25.525	−16.926	0.946	23.001	−16.992	0.878	38.867	−30.736
NUK_U	0.935	21.446	−12.884	0.912	21.029	−7.167	0.895	28.695	−17.973	0.897	26.484	−15.703	0.838	35.497	−23.021
QAS_A	0.965	18.721	−13.895	0.941	19.458	−10.166	0.935	21.590	−13.307	0.941	20.643	−13.268	0.916	23.397	−14.076
QAS_L	0.964	21.793	−17.481	0.944	21.902	−15.399	0.940	24.508	−18.202	0.860	30.825	−19.469	0.914	32.302	−26.107
QAS_M	0.954	19.928	−13.629	0.925	21.384	−12.545	0.924	22.950	−13.826	0.686	39.781	−18.695	0.909	26.443	−17.937
QAS_U	0.882	26.996	−13.860	0.885	24.418	−10.218	0.854	28.579	−12.772	0.783	33.375	−15.156	0.832	30.976	−16.604
SCO_L	0.941	45.047	−42.080	0.946	57.995	−55.597	0.931	46.659	−43.418	0.848	49.158	−42.388	0.903	52.096	−48.035
SCO_U	0.955	29.401	−25.827	0.956	38.942	−36.141	0.947	33.949	−30.402	0.854	37.636	−28.797	0.919	38.922	−34.348
TAS_A	0.832	23.914	−5.388	0.820	33.548	−21.545	0.784	28.998	−13.563	0.555	39.720	−15.553	0.770	50.083	−41.663
TAS_L	0.890	24.731	−16.127	0.846	37.331	−28.296	0.844	30.939	−22.382	0.669	41.020	−26.273	0.806	60.176	−54.559
TAS_U	0.843	26.555	−13.816	0.831	36.728	−25.469	0.811	31.254	−20.427	0.821	32.155	−21.913	0.790	59.408	−53.016
THU_L	0.941	19.406	−8.230	0.901	30.903	−15.534	0.911	30.105	−18.935	0.832	30.930	−12.779	0.887	35.719	−26.213
THU_U	0.920	21.676	−7.252	0.869	33.746	−13.927	0.887	31.607	−17.470	0.910	22.320	−8.726	0.867	35.569	−24.288
UPE_L	0.927	31.492	−24.924	0.920	35.161	−28.341	0.903	44.121	−38.393	0.825	43.079	−33.108	0.846	55.193	−48.745
UPE_U	0.944	19.687	−11.110	0.941	20.758	−10.519	0.919	30.271	−23.061	0.905	26.428	−16.312	0.873	36.549	−27.726
THU_U2	0.924	21.034	−7.189	0.896	30.470	−8.453	0.878	32.192	−17.356	0.659	41.806	−15.269	0.860	37.892	−26.263
S5	0.935	19.169	−5.092	0.921	25.615	−14.944	0.905	25.548	−13.036	0.923	22.827	−14.295	0.846	41.005	−31.708
S6	0.942	16.190	−4.437	0.931	19.888	−7.279	0.899	23.449	−9.295	0.919	19.253	−7.255	0.834	35.794	−23.832
S9	0.935	21.199	−13.751	0.924	21.525	−10.368	0.891	27.131	−14.897	0.906	22.673	−12.683	0.808	36.076	−21.946

Note: Unit for both RMSE and BIAS, $W \cdot m^{-2}$.

Table S5 Daily data evaluation indexes of LWU for five reanalysis datasets for all stations

LWU	ERA5			ERA-Interim			JRA55			MERRA-2			NCEP2		
	R	RMSE	BIAS	*R*	RMSE	BIAS	*R*	RMSE	BIAS	*R*	RMSE	BIAS	*R*	RMSE	BIAS
CEN	0.988	7.821	2.225	0.984	14.006	11.416	0.978	22.437	20.020	0.749	57.466	−48.444	0.950	29.350	25.988
EGP	0.974	10.496	1.001	0.975	10.924	4.612	0.969	15.579	7.422	0.716	62.427	−54.050	0.920	21.758	13.097
KAN_L	0.971	11.876	−3.786	0.965	14.204	−7.732	0.982	6.853	0.746	0.735	51.934	−40.980	0.895	21.601	−12.604
KAN_M	0.981	9.107	0.581	0.973	9.443	1.691	0.974	13.344	8.721	0.758	46.256	−34.069	0.919	16.288	−1.656
KAN_U	0.982	9.246	−2.014	0.977	9.003	0.299	0.975	11.510	5.708	0.731	52.051	−39.974	0.914	16.832	1.206
KPC_L	0.979	22.751	−20.002	0.980	14.914	−11.676	0.971	12.601	−6.980	0.752	62.722	−53.508	0.932	19.661	−10.640
KPC_U	0.984	9.208	−4.031	0.979	9.498	0.071	0.976	10.512	0.219	0.749	52.318	−39.429	0.944	15.421	−1.039
MIT	0.750	23.517	6.313	0.862	17.971	9.383	0.742	29.923	13.529	0.417	44.397	−21.395	0.679	29.702	−15.776
NUK_K	0.933	11.662	3.147	0.938	11.076	2.526	0.951	12.883	8.428	0.738	45.058	−36.997	0.881	13.989	0.359
NUK_L	0.961	16.745	−12.844	0.959	15.909	−11.674	0.963	13.003	−9.352	0.731	54.796	−44.657	0.895	21.972	−15.006
NUK_N	0.974	10.575	−5.997	0.968	8.995	−2.258	0.978	7.441	1.160	0.805	38.248	−25.922	0.917	16.391	−7.983
NUK_U	0.929	13.451	−4.497	0.928	13.371	−2.270	0.942	11.496	0.184	0.783	46.084	−36.016	0.879	17.633	−4.070
QAS_A	0.943	11.401	−4.512	0.917	13.040	1.676	0.937	12.054	4.266	0.831	53.309	−46.825	0.860	19.535	9.909
QAS_L	0.967	10.601	−7.666	0.949	8.796	1.006	0.963	7.095	−2.607	0.636	48.868	−35.931	0.877	12.397	−0.882
QAS_M	0.966	8.835	−5.425	0.950	10.028	3.509	0.967	7.435	0.845	0.631	61.373	−52.615	0.890	14.284	4.212
QAS_U	0.951	9.566	−2.398	0.933	12.382	5.354	0.945	11.654	5.045	0.657	47.168	−33.928	0.869	18.375	8.661
SCO_L	0.938	50.923	−48.455	0.941	57.141	−53.191	0.949	20.567	−16.479	0.726	73.982	−66.193	0.932	20.564	−15.020
SCO_U	0.950	44.565	−42.235	0.956	46.343	−42.970	0.969	15.817	−11.977	0.722	70.683	−62.340	0.957	15.822	−10.843
TAS_A	0.946	8.890	−2.489	0.910	15.169	−6.926	0.906	15.411	8.214	0.544	56.328	−46.830	0.898	20.476	−15.686
TAS_L	0.938	9.679	−5.754	0.892	18.745	−11.869	0.848	13.826	4.608	0.463	50.474	−36.084	0.864	27.187	−22.949
TAS_U	0.953	8.242	−3.508	0.916	17.182	−9.664	0.909	14.845	7.569	0.663	34.250	−19.990	0.900	23.722	−19.445
THU_L	0.977	16.822	−9.587	0.954	14.897	−1.274	0.978	10.000	−3.028	0.755	55.033	−44.656	0.940	18.216	−7.087
THU_U	0.972	17.493	−8.421	0.944	16.673	1.221	0.977	9.533	0.177	0.847	46.098	−37.091	0.939	17.160	−3.464
UPE_L	0.970	14.372	−9.582	0.950	15.467	−8.330	0.959	12.515	−5.911	0.725	58.825	−47.569	0.903	20.507	−10.912
UPE_U	0.984	8.548	−4.711	0.961	13.498	−5.393	0.983	8.196	−0.251	0.736	57.846	−46.521	0.945	13.420	−2.420
THU_U2	0.974	14.780	−5.112	0.960	15.071	1.522	0.973	10.444	1.948	0.657	60.846	−48.284	0.935	18.348	−3.249
S5	0.968	12.988	−3.990	0.968	13.675	−7.289	0.981	7.176	2.040	0.786	38.758	−25.634	0.887	21.722	−11.588
S6	0.985	8.457	3.910	0.971	9.575	0.682	0.975	11.184	6.427	0.810	33.179	−18.401	0.915	17.184	−5.046
S9	0.982	8.424	−1.569	0.975	9.153	2.397	0.976	12.703	8.458	0.803	34.885	−19.932	0.920	16.432	−0.733

Note: Unit for both RMSE and BIAS, $W \cdot m^{-2}$.

Table S6 Monthly data evaluation indexes of SWD for five reanalysis datasets for all stations

SWD	ERA5			ERA-Interim			JRA55			MERRA-2			NCEP2		
	R	RMSE	BIAS	*R*	RMSE	BIAS	*R*	RMSE	BIAS	*R*	RMSE	BIAS	*R*	RMSE	BIAS
CEN	0.997	16.422	−9.646	0.994	35.742	−29.402	0.995	24.744	−16.649	0.995	31.071	−24.222	0.997	12.532	−4.232
EGP	0.998	8.008	−1.305	0.997	11.058	−2.074	0.996	13.563	5.111	0.995	14.982	−8.660	0.996	15.099	7.247
KAN_L	0.994	24.050	−14.870	0.997	9.712	−4.461	0.996	15.811	−8.425	0.996	18.455	−12.626	0.996	20.927	14.472
KAN_M	0.996	11.402	1.000	0.994	15.013	−7.251	0.996	13.847	−6.331	0.994	22.394	−15.400	0.995	12.651	4.178
KAN_U	0.998	9.452	−3.968	0.995	13.762	−6.302	0.997	14.023	−6.779	0.997	20.940	−15.640	0.998	9.202	3.117
KPC_L	0.992	14.395	4.755	0.991	15.767	−1.242	0.989	20.788	−14.262	0.986	19.165	−9.620	0.988	17.795	5.995
KPC_U	0.984	18.265	−0.491	0.992	19.463	−14.449	0.984	25.676	−16.995	0.977	28.037	−17.319	0.978	22.067	1.686
MIT	0.992	26.223	−15.785	0.992	15.214	2.906	0.993	12.969	2.274	0.992	18.447	−9.969	0.988	44.210	35.091
NUK_K	0.966	25.520	−4.964	0.991	14.335	−3.236	0.982	17.968	4.655	0.985	20.271	−9.439	0.985	44.501	35.295
NUK_L	0.994	16.257	10.624	0.992	13.030	2.099	0.993	19.412	13.671	0.990	13.941	1.024	0.989	36.076	27.399

Continued

SWD	ERA5			ERA-Interim			JRA55			MERRA-2			NCEP2		
	R	RMSE	BIAS	*R*	RMSE	BIAS	*R*	RMSE	BIAS	*R*	RMSE	BIAS	*R*	RMSE	BIAS
NUK_N	0.995	20.142	−13.322	0.996	11.038	−5.628	0.997	10.510	−4.692	0.995	17.992	−11.746	0.997	22.240	17.426
NUK_U	0.973	26.209	6.943	0.973	25.348	−7.330	0.972	25.075	3.729	0.971	26.082	−6.744	0.975	29.261	13.597
QAS_A	0.994	11.935	−2.042	0.991	19.442	−12.552	0.989	20.781	−8.849	0.994	20.265	−13.817	0.992	13.698	2.329
QAS_L	0.993	14.330	7.390	0.990	15.220	1.589	0.992	12.381	2.747	0.988	15.485	−4.701	0.988	30.208	20.390
QAS_M	0.975	22.328	6.631	0.996	10.575	−5.113	0.975	20.901	−0.014	0.976	20.980	−4.752	0.976	27.531	13.276
QAS_U	0.990	14.973	−0.479	0.990	18.608	−9.935	0.989	19.679	−8.529	0.991	21.755	−14.022	0.993	13.511	3.913
SCO_L	0.989	43.100	35.268	0.991	33.007	24.174	0.989	32.378	25.922	0.986	27.786	18.639	0.989	41.340	34.197
SCO_U	0.991	26.016	17.916	0.991	20.848	9.292	0.992	18.563	10.988	0.988	17.915	3.063	0.992	24.585	17.507
TAS_A	0.992	15.289	−3.626	0.994	18.989	−13.537	0.994	18.109	−10.844	0.991	25.851	−18.479	0.994	20.436	13.744
TAS_L	0.993	13.766	5.398	0.993	13.672	1.403	0.994	11.905	0.178	0.989	15.471	−4.404	0.987	37.939	29.798
TAS_U	0.978	22.370	3.306	0.974	24.531	−1.952	0.974	24.010	−2.799	0.972	26.059	−7.975	0.974	37.024	22.969
THU_L	0.996	20.278	−16.453	0.995	29.500	−24.652	0.995	12.582	−5.865	0.993	28.492	−24.036	0.992	22.703	15.054
THU_U	0.995	21.404	−16.423	0.993	32.900	−26.817	0.996	15.102	−8.752	0.995	31.127	−26.236	0.996	16.992	11.084
UPE_L	0.993	12.116	−3.859	0.994	11.552	−2.585	0.991	16.494	9.078	0.990	15.650	−7.883	0.988	35.603	25.980
UPE_U	0.998	12.042	−6.319	0.997	17.595	−14.538	0.997	8.487	−1.638	0.995	22.162	−17.233	0.995	17.008	10.340
THU_U2	0.989	37.436	−32.159	0.981	58.365	−49.787	0.995	27.912	−22.817	0.988	47.699	−42.440	0.998	8.550	4.388
S5	0.993	19.133	−9.503	0.996	10.583	0.454	0.994	13.740	−4.395	0.995	14.287	−7.198	0.993	28.217	18.493
S6	0.997	9.042	−0.108	0.996	12.891	−7.107	0.997	9.962	−3.774	0.995	19.780	−13.353	0.996	15.455	7.795
S9	0.998	9.518	−5.352	0.997	13.513	−9.586	0.998	15.938	−10.378	0.997	25.154	−19.004	0.998	7.994	−0.953

Note: Unit for both RMSE and BIAS, $W \cdot m^{-2}$.

Table S7 Monthly data evaluation indexes of SWU for five reanalysis datasets for all stations

SWU	ERA5			ERA-Interim			JRA55			MERRA-2			NCEP2		
	R	RMSE	BIAS	*R*	RMSE	BIAS	*R*	RMSE	BIAS	*R*	RMSE	BIAS	*R*	RMSE	BIAS
CEN	0.988	14.980	−2.218	0.956	45.496	−35.402	0.981	18.030	3.969	0.991	30.386	−24.377	0.971	40.538	−28.013
EGP	0.999	10.925	7.853	0.997	8.520	−2.924	0.998	30.875	25.481	0.997	12.418	−8.801	0.998	17.263	13.756
KAN_L	0.757	59.534	−41.806	0.968	25.383	11.448	0.974	49.967	36.607	0.976	37.344	−28.568	0.963	55.864	39.544
KAN_M	0.926	45.431	22.621	0.917	38.880	8.993	0.936	45.109	24.714	0.968	27.992	−14.746	0.929	33.509	7.045
KAN_U	0.996	10.999	3.392	0.991	16.295	1.285	0.996	15.588	10.407	0.994	28.897	−22.962	0.996	11.716	5.673
KPC_L	0.810	74.499	54.386	0.809	62.115	35.540	0.856	66.223	50.247	0.884	38.763	15.857	0.811	68.962	48.790
KPC_U	0.966	26.083	12.941	0.948	27.249	−1.176	0.975	22.342	11.929	0.991	30.115	−27.549	0.969	21.427	6.471
MIT	0.692	71.410	−48.388	0.902	31.426	0.966	0.888	64.315	44.453	0.933	44.124	−27.553	0.899	55.893	38.937
NUK_K	0.583	63.739	−41.134	0.932	42.074	−27.507	0.911	53.401	40.491	0.864	67.701	−50.875	0.931	36.441	25.413
NUK_L	0.903	58.528	44.916	0.933	41.214	29.238	0.876	93.689	73.682	0.940	16.608	3.291	0.861	69.202	51.429
NUK_N	0.972	30.784	−20.797	0.893	37.444	11.867	0.842	67.004	43.175	0.966	40.768	−26.469	0.816	57.005	28.938
NUK_U	0.936	43.981	24.920	0.956	21.318	−4.954	0.943	48.349	30.642	0.975	29.560	−20.551	0.943	28.053	9.117
QAS_A	0.983	19.744	7.356	0.976	42.806	−33.307	0.977	21.378	8.618	0.970	40.970	−29.289	0.965	45.435	−33.735
QAS_L	0.819	47.228	29.995	0.727	38.695	−2.968	0.702	84.407	58.013	0.871	29.622	−8.328	0.796	33.792	0.888
QAS_M	0.869	37.136	14.219	0.852	41.749	−20.939	0.839	54.348	31.445	0.942	36.379	−22.373	0.881	42.698	−25.545
QAS_U	0.922	33.789	13.294	0.936	44.655	−30.944	0.919	41.238	21.848	0.961	44.555	−30.737	0.936	47.543	−33.203
SCO_L	0.796	107.687	84.359	0.777	97.547	70.897	0.811	109.993	87.828	0.854	68.917	50.117	0.860	75.527	60.395
SCO_U	0.849	80.346	58.436	0.841	71.102	44.923	0.859	84.857	64.207	0.908	43.387	24.842	0.901	50.563	35.552
TAS_A	0.939	38.636	19.300	0.956	27.550	−12.837	0.947	38.331	21.276	0.978	45.872	−34.815	0.955	43.951	−28.657
TAS_L	0.802	60.239	38.378	0.813	44.709	17.569	0.767	79.339	55.616	0.934	25.696	−7.770	0.778	40.283	1.259

Continued

SWU	ERA5			ERA-Interim			JRA55			MERRA-2			NCEP2		
	R	RMSE	BIAS	*R*	RMSE	BIAS	*R*	RMSE	BIAS	*R*	RMSE	BIAS	*R*	RMSE	BIAS
TAS_U	0.884	49.757	28.241	0.895	31.956	2.430	0.876	58.403	36.064	0.960	30.100	−19.509	0.885	32.705	−8.150
THU_L	0.961	38.072	−30.486	0.866	61.432	−46.929	0.873	58.687	42.299	0.966	46.126	−37.048	0.962	30.781	18.801
THU_U	0.949	45.753	−38.737	0.840	75.877	−63.860	0.950	35.241	25.011	0.965	60.424	−53.716	0.972	19.898	−0.970
UPE_L	0.983	16.879	−11.593	0.975	14.689	−2.841	0.942	62.017	50.009	0.989	35.183	−30.186	0.964	35.725	27.474
UPE_U	0.958	24.225	8.513	0.941	27.473	−9.254	0.932	50.979	34.427	0.981	27.890	−20.380	0.954	28.929	14.567
THU_U2	0.933	71.891	−66.605	0.778	112.682	−102.436	0.968	21.587	10.196	0.939	86.137	−81.179	0.971	28.971	−18.289
S5	0.679	61.540	−40.437	0.983	21.472	10.375	0.988	45.459	32.521	0.971	38.622	−27.789	0.979	55.742	38.719
S6	0.954	29.009	11.226	0.945	28.321	2.629	0.948	44.034	24.810	0.977	29.673	−18.366	0.943	35.959	15.231
S9	0.983	23.861	10.269	0.978	23.824	4.305	0.986	25.024	13.675	0.995	25.318	−18.437	0.984	16.683	0.510

Note: Unit for both RMSE and BIAS, $W \cdot m^{-2}$.

Table S8 Monthly data evaluation indexes of LWD for five reanalysis datasets for all stations

LWD	ERA5			ERA-Interim			JRA55			MERRA-2			NCEP2		
	R	RMSE	BIAS	*R*	RMSE	BIAS	*R*	RMSE	BIAS	*R*	RMSE	BIAS	*R*	RMSE	BIAS
CEN	0.951	26.025	−21.536	0.960	27.331	−16.990	0.932	29.016	−16.842	0.857	29.931	−24.158	0.951	22.252	−15.986
EGP	0.943	24.905	−21.802	0.936	27.561	−24.470	0.935	36.111	−34.257	0.768	37.764	−32.674	0.915	38.189	−36.397
KAN_L	0.985	12.114	−5.863	0.978	18.374	−15.495	0.983	18.531	−13.995	0.935	20.615	−17.065	0.968	33.392	−32.398
KAN_M	0.992	11.475	−10.695	0.988	11.622	−9.644	0.980	16.525	−12.554	0.930	17.059	−12.903	0.955	25.079	−23.342
KAN_U	0.986	14.600	−13.783	0.979	14.703	−12.724	0.977	22.856	−19.961	0.908	21.219	−17.552	0.937	23.101	−20.464
KPC_L	0.977	15.281	−12.539	0.985	13.375	−9.395	0.967	23.584	−20.815	0.918	25.144	−19.216	0.962	27.862	−25.361
KPC_U	0.981	15.825	−14.218	0.978	8.959	−4.959	0.970	23.529	−21.009	0.897	25.651	−20.141	0.959	26.224	−24.138
MIT	0.949	11.952	−7.510	0.822	14.039	−6.791	0.936	17.253	−15.420	0.794	20.245	−14.712	0.936	50.744	−50.064
NUK_K	0.904	18.380	−0.704	0.968	19.404	−6.454	0.891	20.811	−10.066	0.882	16.072	−8.875	0.888	29.886	−26.845
NUK_L	0.986	21.603	−20.818	0.969	19.478	−17.519	0.977	29.428	−27.549	0.911	29.663	−26.511	0.966	36.414	−35.415
NUK_N	0.992	16.766	−15.554	0.987	9.954	−8.421	0.989	20.229	−17.371	0.987	17.828	−16.974	0.980	31.657	−30.943
NUK_U	0.982	12.775	−11.426	0.966	10.134	−5.713	0.966	19.885	−16.836	0.965	16.625	−14.537	0.958	23.204	−21.466
QAS_A	0.983	14.601	−13.694	0.979	11.668	−9.633	0.984	15.220	−13.463	0.977	14.266	−13.180	0.969	15.601	−14.289
QAS_L	0.986	18.618	−17.493	0.973	16.987	−15.370	0.981	19.702	−18.285	0.914	22.816	−19.577	0.976	27.069	−26.167
QAS_M	0.992	14.064	−13.140	0.988	11.708	−10.970	0.986	14.842	−13.227	0.799	25.106	−18.399	0.983	17.962	−17.058
QAS_U	0.891	18.675	−12.121	0.907	15.425	−9.169	0.884	19.071	−11.013	0.835	21.123	−13.294	0.864	20.935	−14.756
SCO_L	0.979	43.067	−41.920	0.978	56.227	−55.556	0.986	43.840	−43.346	0.919	44.943	−42.403	0.980	48.642	−47.902
SCO_U	0.987	26.936	−25.893	0.982	37.038	−36.294	0.991	30.811	−30.407	0.914	32.369	−29.032	0.985	34.996	−34.368
TAS_A	0.784	15.446	−4.462	0.768	25.952	−20.451	0.764	19.786	−12.347	0.601	24.226	−14.797	0.760	43.568	−40.329
TAS_L	0.924	16.291	−13.888	0.883	27.816	−25.416	0.916	22.317	−20.506	0.719	29.118	−24.662	0.913	53.190	−52.301
TAS_U	0.860	16.567	−11.490	0.835	27.335	−23.276	0.852	22.007	−18.407	0.851	23.189	−19.703	0.852	52.591	−50.911
THU_L	0.987	10.986	−8.242	0.959	22.710	−15.121	0.982	22.805	−18.998	0.912	21.389	−13.722	0.975	27.588	−25.974
THU_U	0.973	13.008	−7.509	0.934	25.533	−14.204	0.966	23.881	−17.718	0.979	11.825	−8.749	0.965	26.911	−24.418
UPE_L	0.982	25.909	−24.186	0.980	29.096	−27.571	0.982	38.933	−37.815	0.911	35.986	−32.763	0.963	49.373	−48.425
UPE_U	0.988	12.396	−10.623	0.983	12.991	−10.131	0.985	23.871	−22.606	0.987	16.958	−15.906	0.976	28.678	−27.494
THU_U2	0.975	12.650	−7.203	0.961	22.459	−8.860	0.960	24.285	−17.280	0.769	30.258	−15.879	0.968	28.818	−26.172
S5	0.974	12.993	−5.220	0.969	18.371	−15.002	0.971	18.491	−13.148	0.967	16.679	−14.252	0.967	32.709	−31.550
S6	0.981	8.501	−4.647	0.977	11.597	−7.451	0.966	15.623	−9.612	0.972	10.409	−7.372	0.952	25.611	−23.726
S9	0.972	15.477	−13.731	0.964	14.175	−10.361	0.951	20.551	−15.075	0.957	15.252	−12.613	0.928	24.899	−21.927

Note: Unit for both RMSE and BIAS, $W \cdot m^{-2}$.

Table S9 Monthly data evaluation indexes of LWU for five reanalysis datasets for all stations

LWU	ERA5			ERA-Interim			JRA55			MERRA-2			NCEP2		
	R	RMSE	BIAS	*R*	RMSE	BIAS	*R*	RMSE	BIAS	*R*	RMSE	BIAS	*R*	RMSE	BIAS
CEN	0.999	3.881	1.993	0.998	12.050	11.630	0.997	20.383	19.854	0.838	53.249	−48.723	0.996	26.324	25.867
EGP	0.996	4.387	0.943	0.994	6.412	4.661	0.996	11.050	7.200	0.796	59.395	−54.599	0.986	16.334	12.935
KAN_L	0.987	9.144	−3.799	0.983	11.149	−7.767	0.997	2.479	0.766	0.757	48.525	−40.961	0.980	13.976	−12.564
KAN_M	0.994	5.671	0.621	0.989	5.315	1.715	0.995	10.125	8.738	0.775	42.140	−33.926	0.985	6.788	−1.659
KAN_U	0.996	6.158	−2.164	0.993	4.691	0.131	0.997	7.241	5.537	0.756	49.336	−41.518	0.985	6.804	1.102
KPC_L	0.994	21.173	−20.030	0.995	12.613	−11.668	0.991	8.905	−7.053	0.809	59.723	−54.094	0.988	12.471	−10.585
KPC_U	0.996	5.546	−3.980	0.994	4.679	0.150	0.996	5.112	0.301	0.767	49.997	−40.011	0.992	6.186	−0.925
MIT	0.806	16.874	5.545	0.920	14.132	9.215	0.816	23.351	12.844	0.450	35.645	−21.516	0.778	23.365	−16.571
NUK_K	0.964	8.146	3.579	0.970	7.038	2.964	0.983	10.268	8.505	0.860	39.798	−37.333	0.970	6.882	0.220
NUK_L	0.990	14.081	−12.380	0.993	12.654	−11.185	0.989	10.304	−9.148	0.751	52.622	−46.029	0.983	15.645	−14.838
NUK_N	0.989	8.551	−6.291	0.993	4.187	−2.201	0.996	3.037	1.254	0.815	34.700	−24.827	0.989	9.189	−7.964
NUK_U	0.960	8.704	−4.014	0.962	8.371	−1.911	0.967	7.121	0.574	0.793	43.430	−37.095	0.957	8.818	−3.585
QAS_A	0.995	4.065	−2.542	0.980	6.340	3.446	0.997	7.522	6.210	0.962	47.360	−46.849	0.984	16.591	12.588
QAS_L	0.988	8.941	−7.559	0.989	3.563	0.976	0.989	3.799	−2.534	0.629	44.139	−35.669	0.972	7.229	−0.779
QAS_M	0.988	6.527	−5.579	0.991	5.522	3.711	0.993	3.469	0.835	0.743	56.076	−53.516	0.974	10.400	4.383
QAS_U	0.982	5.345	−2.057	0.970	8.331	5.329	0.980	8.199	5.389	0.666	41.788	−33.529	0.961	14.992	9.222
SCO_L	0.976	49.540	−48.495	0.973	56.114	−53.390	0.974	18.464	−16.497	0.773	71.107	−66.500	0.977	17.213	−15.021
SCO_U	0.986	43.227	−42.401	0.985	45.320	−43.207	0.990	13.717	−11.955	0.763	67.904	−62.730	0.991	12.740	−10.823
TAS_A	0.974	5.551	−2.180	0.950	11.090	−6.401	0.961	12.280	8.543	0.661	49.875	−46.989	0.966	16.622	−15.389
TAS_L	0.987	6.013	−5.367	0.962	14.023	−11.014	0.926	9.088	4.570	0.455	45.167	−36.687	0.970	23.231	−22.185
TAS_U	0.992	4.154	−3.124	0.968	12.788	−9.281	0.959	11.330	7.542	0.630	32.179	−21.279	0.977	20.134	−19.118
THU_L	0.992	14.147	−9.376	0.976	10.467	−1.086	0.994	6.058	−2.973	0.837	51.657	−46.712	0.984	10.685	−6.719
THU_U	0.991	14.717	−8.492	0.971	12.012	1.032	0.994	5.214	0.161	0.904	41.757	−37.266	0.985	9.100	−3.539
UPE_L	0.980	12.554	−9.545	0.963	13.110	−8.304	0.986	8.456	−5.891	0.762	54.810	−47.529	0.974	13.575	−10.910
UPE_U	0.996	5.637	−4.746	0.977	10.287	−5.346	0.997	4.312	−0.243	0.763	54.119	−46.549	0.991	6.423	−2.476
THU_U2	0.993	11.401	−5.097	0.987	9.470	1.002	0.993	5.623	1.995	0.776	55.284	−48.850	0.985	9.320	−3.163
S5	0.981	10.660	−4.065	0.986	10.670	−7.354	0.992	4.310	2.073	0.778	36.433	−25.631	0.978	13.214	−11.521
S6	0.996	5.600	3.974	0.987	5.552	0.633	0.994	7.917	6.519	0.787	31.067	−18.768	0.982	8.186	−4.871
S9	0.994	5.193	−1.434	0.990	5.360	2.532	0.994	9.857	8.591	0.778	32.508	−19.658	0.984	6.197	−0.585

Note: Unit for both RMSE and BIAS, $W \cdot m^{-2}$.